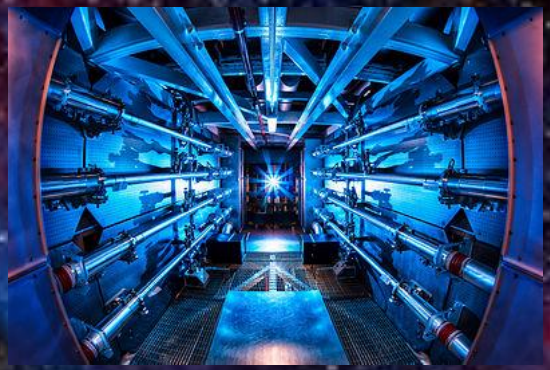

Energetic particles in laser-plasmas & astrophysics

Tony Bell
Oxford/RAL

SN1006: A supernova remnant 7,000 light years from Earth
X-ray (blue): NASA/CXC/Rutgers/G.Cassam-Chenai, J.Hughes et al; Radio (red): NRAO/AUI/GBT/VLA/Dyer, Maddalena & Cornwell; Optical (yellow/orange): Middlebury College/F.Winkler. NOAO/AURA/NSF/CTIO Schmidt & DSS

Energetic particles in astrophysics

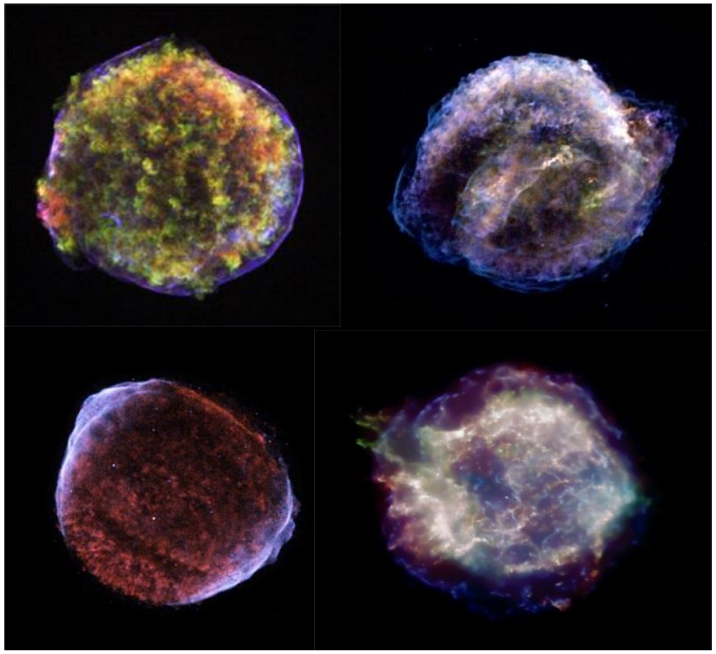

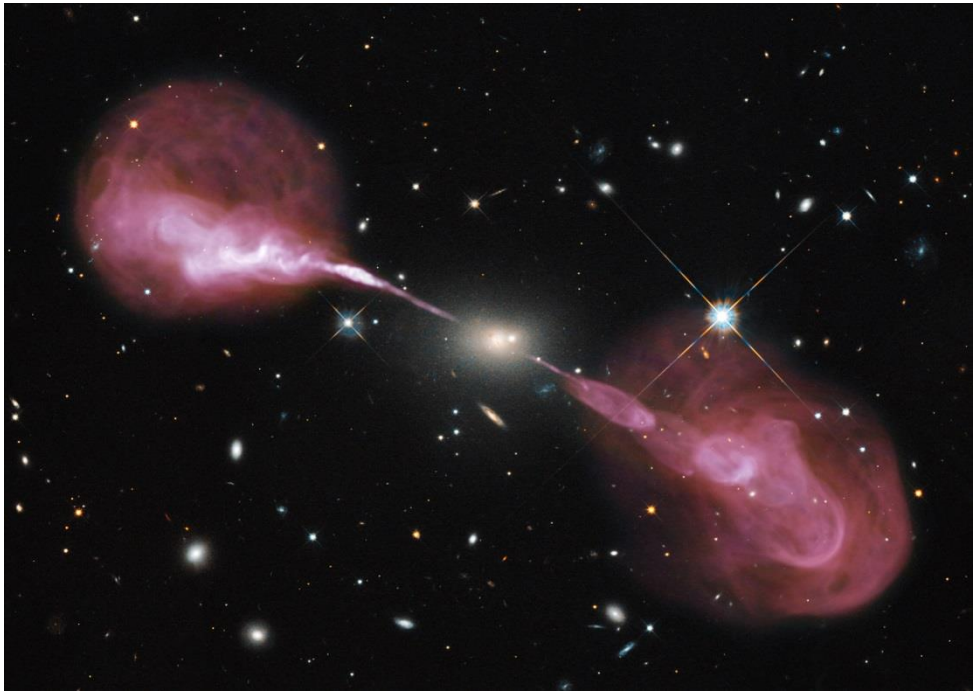

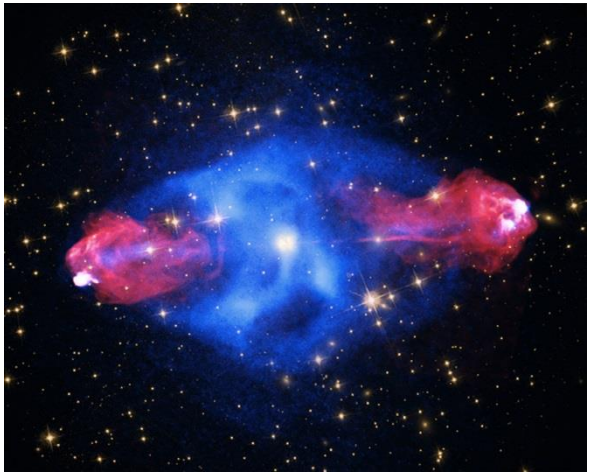

CR populations

(Nagano & Watson 2000)

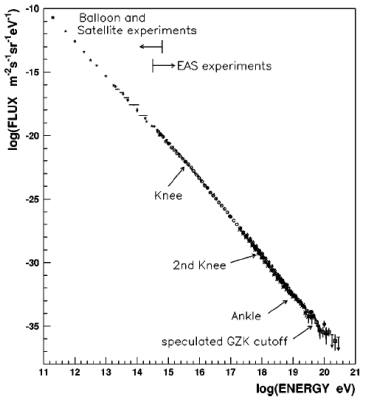

(I) Galactic Supernova remnants

(II) Probably galactic

(III) Extra-galactic ?

knee

ankle

$\sim E^{-2.6}$

$\sim E^{-3}$

log(FLUX * E³ in eV²m⁻²s⁻¹sr⁻¹)

log(ENERGY in eV)

The Auger detector (in Argentina)

30 times size of Paris

Highest energy cosmic rays

One per century per square kilometer

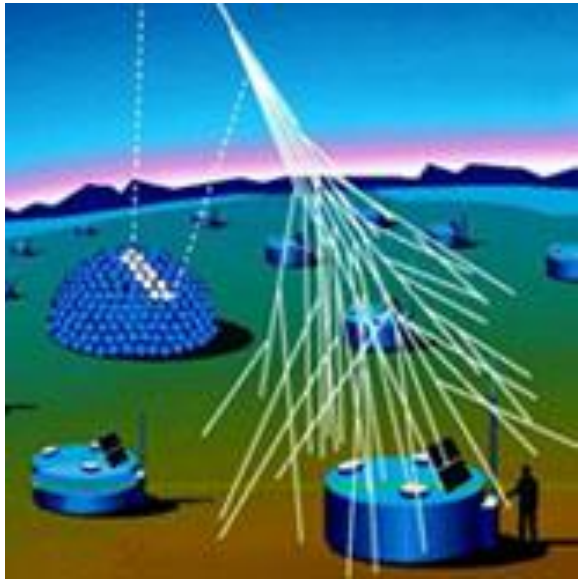

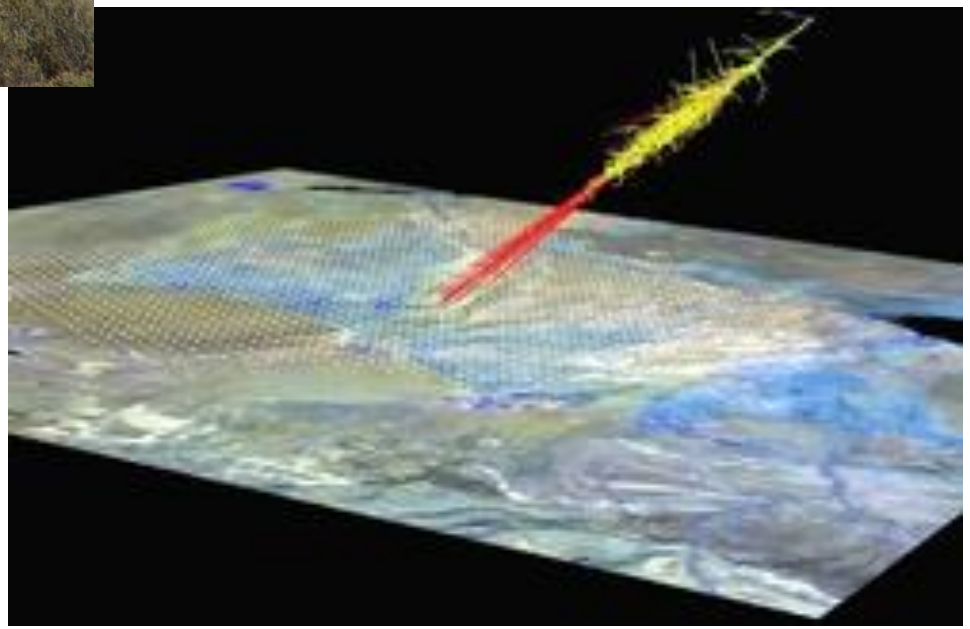

Gamma-ray telescope

HESS γ-ray telescope in Namibia

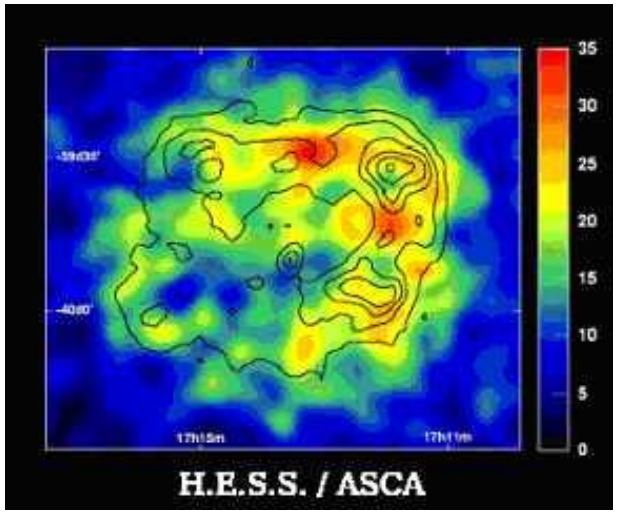

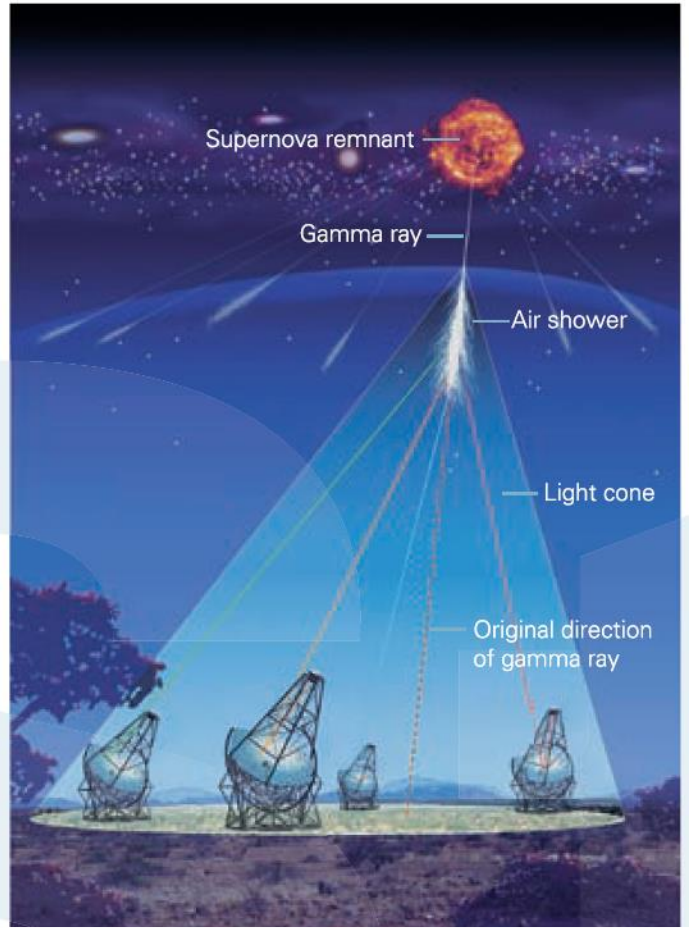

Gamma-rays travel in straight lines!

How do cosmic rays get their energy?

Diffusive shock acceleration

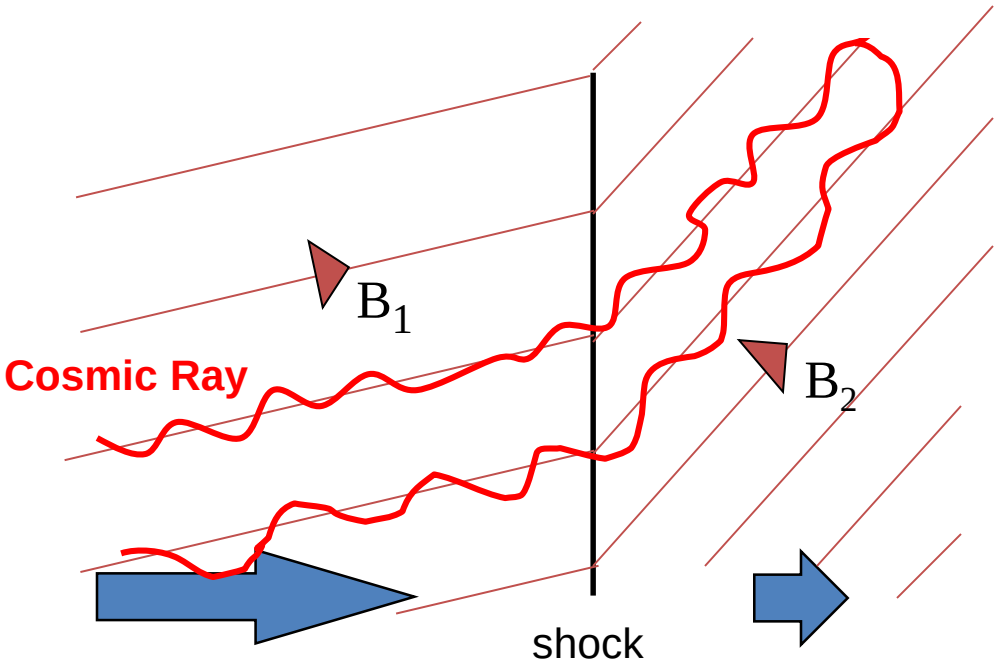

Shock velocity: u_s

CR density at shock: n

At each shock crossing

Fractional energy gain $\frac{\Delta\varepsilon}{\varepsilon} = \frac{u_s}{c}$

Fraction of CR lost $\frac{\Delta n}{n} = -\frac{u_s}{c}$

Differential energy spectrum $N(\varepsilon) \propto \varepsilon^{-2}$

Weibel instability in relativistic shocks

Keshet et al 2009, pair plasma

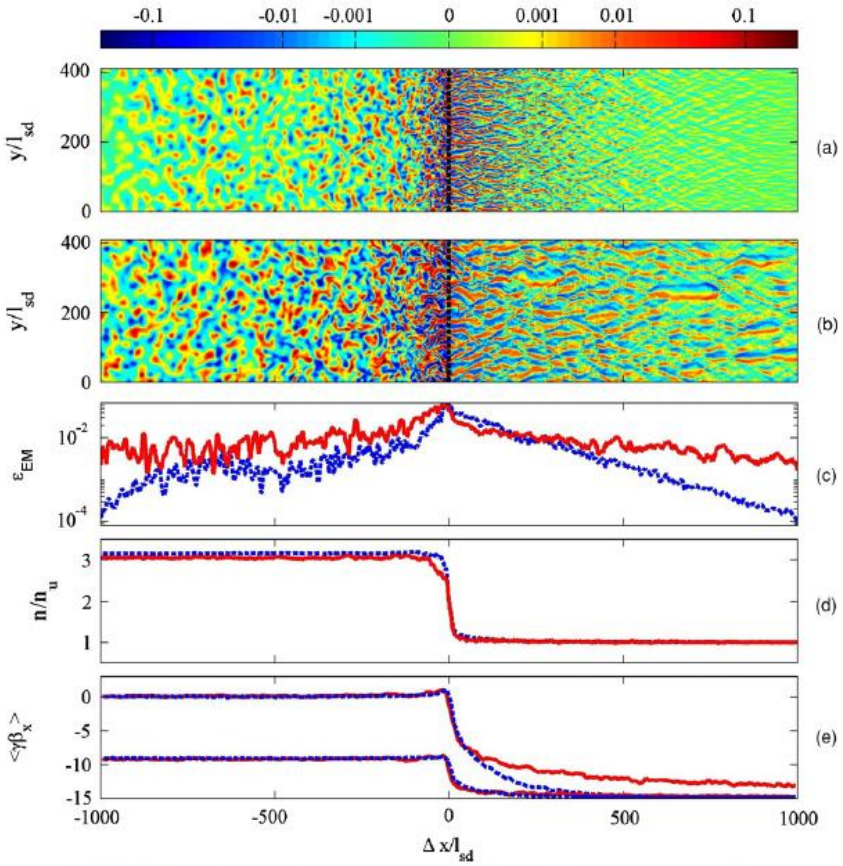

Figure 1. Plasma evolution within $1000 l_{sd}$ of the shock. Normalized transverse magnetic field $\mathrm{sign}(B)\epsilon_B$ (color scale stretched in proportion to $\epsilon_B^{1/4}$ to highlight weak features) is shown at (a) early ($t_1 = 2250\omega_p^{-1}$) and (b) late ($t_2 = 11925\omega_p^{-1}$) times. Here, $\Delta x \equiv x - x_{sh}$ is the distance from the shock, with x_{sh} (dashed) defined as median density between far upstream and far downstream. Also shown are the transverse averages (at t_1, dashed blue, and t_2, solid red) of (c) electromagnetic energy normalized to the upstream kinetic energy $\epsilon_{EM} \equiv [(B^2 + E^2)/8\pi]/[(\gamma_0 - 1)nmc^2]$ (with E the electric field amplitude, included because in the simulation frame the induced $E \sim B$ upstream), (d) density normalized to the far upstream, and (e) particle momentum $\gamma\beta_x$ (with β the velocity in c units) in the x-direction averaged over all particles (higher $\langle\gamma\beta_x\rangle$) and over downstream-headed particles only.

Martins et al 2009, electron ion plasma

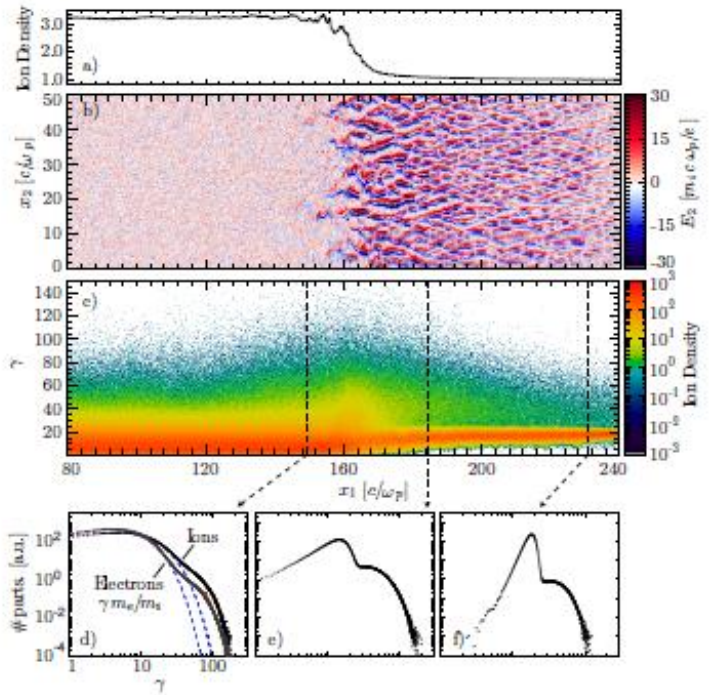

FIG. 1.— Steady state structure of a $m_i/m_e = 32$ collisionless shock at $t = 360/\omega_p$ after first counter-streaming interaction. a) Transverse average of the ion density; b) Transverse electric field; c) Ion energy spectrum along simulation box; d-f) Ion spectra for the downstream, the shock front, and the upstream regions, respectively. The downstream inset includes also the electron spectrum (scaled down by the mass ratio m_e/m_i) with relativistic Maxwellian fits for both species - blue dashed lines -, and a fit to the electron spectrum of a relativistic Maxwellian with a power law trimmed by an exponential cut-off for higher energies - red dotted line.

Weibel instability: opposing energetic electron beams

1) Perturbed beam density

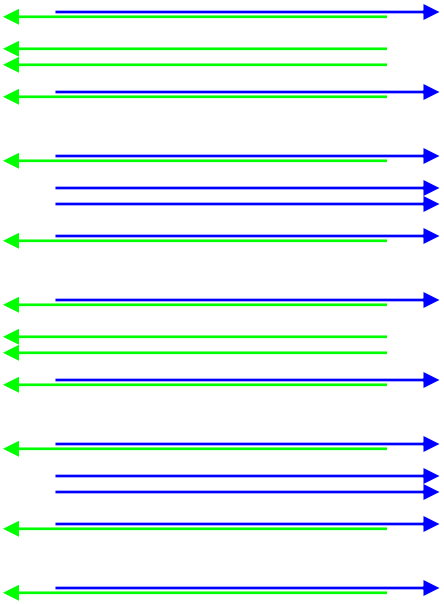

2) Magnetic field

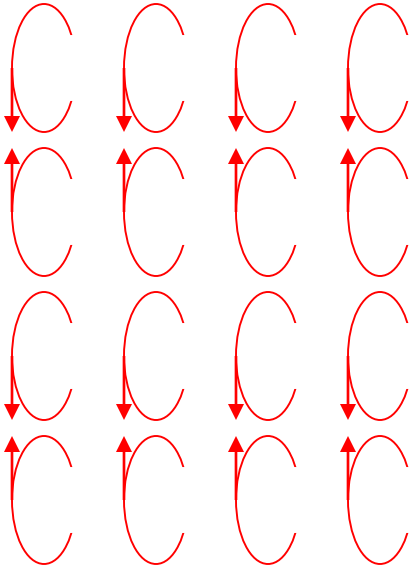

3) Focus currents

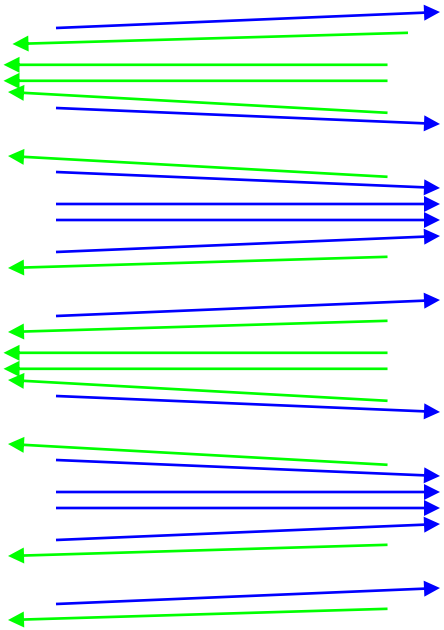

Ramakrishna et al (2009)

Electron beam filamentation

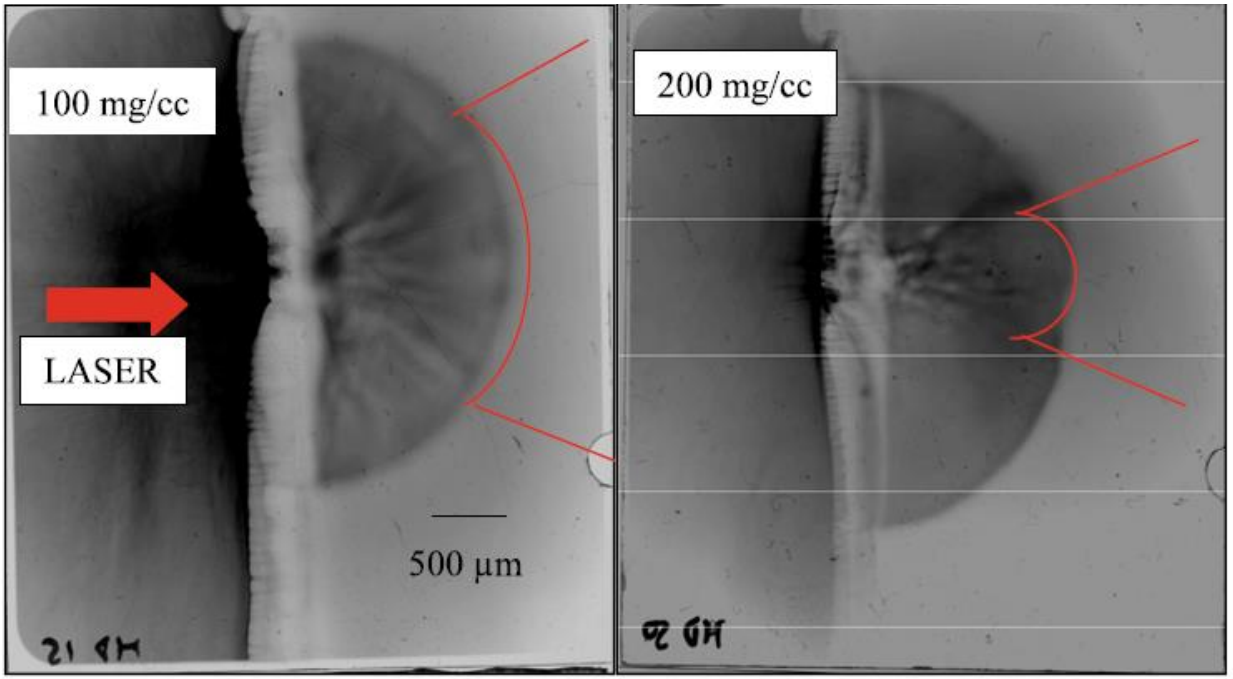

T= 2ps T=2ps

Fig. 3 RCF images of foam targets following CPA interaction. The density of the foam is indicated in figure. Timing relative to the interaction is indicated below the figures. The hemi-circular shadow on the right side of the images is due to the half-washer enclosing the foam (see Fig. 2), while the *vertical white band* at the centre of the images corresponds to the foam-vacuum interface. Beside plasma expansion from the interface into the vacuum, the images clearly show filamentary structures appearing inside the bulk of the target. The cone containing the filaments expanding from the interaction point is indicated by the *red lines* on the right of the figure

Other instabilities in astrophysics

Magnetic field generation

Cassiopeia A

Radio (VLA) | Infrared (Spitzer) | Optical (Hubble) | X-ray (Chandra)

chandra.harvard.edu/photo/0237/0237_radio.jpg

NASA/JPL-Caltech/O Krause(Steward Obs)

NASA/ESA/ Hubble Heritage (STScI/AURA))

NASA/CXC/MIT/UMass Amherst/ M.D.Stage et al.

Mixture of line radiation
& synchrotron continuum

Synchrotron in magnetic field ~ 0.1-1mG
Radio ($h\nu \sim 10^{-5}$eV): electron energy ~1 GeV
X-ray ($h\nu \sim 10^{3}$eV): electron energy ~ 10 TeV

Magnetic field amplification: expanding loops of B

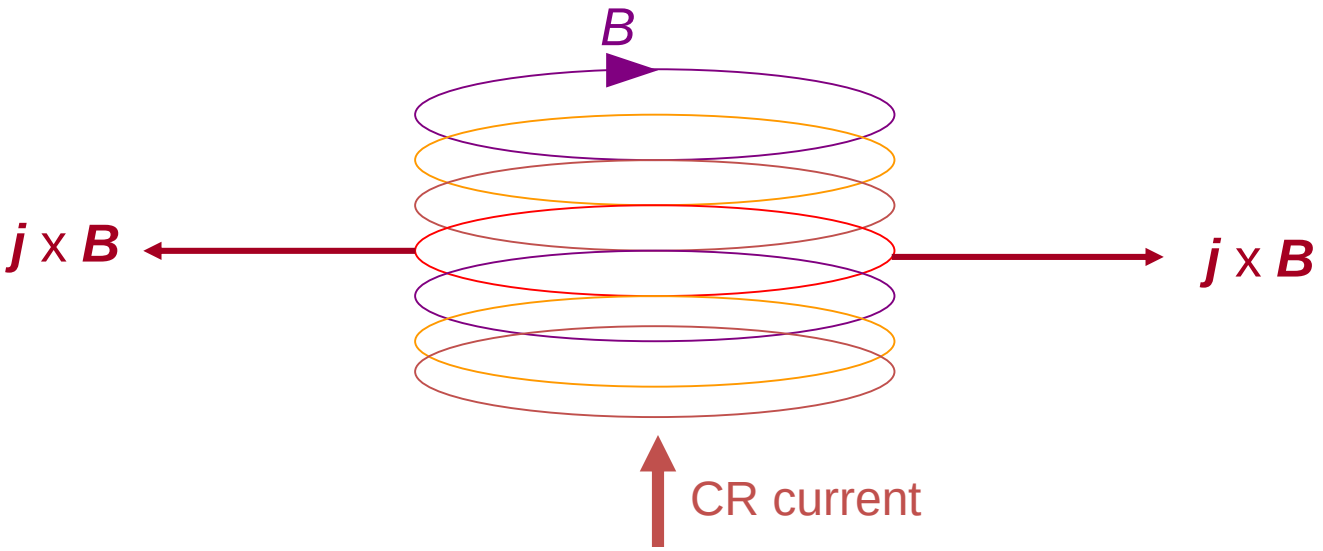

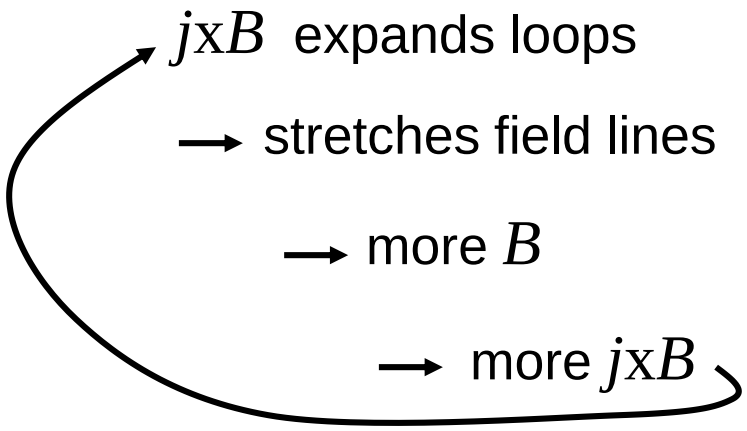

Slice through 3D MHD turbulence driven by current of energetic particles into page

Time sequence

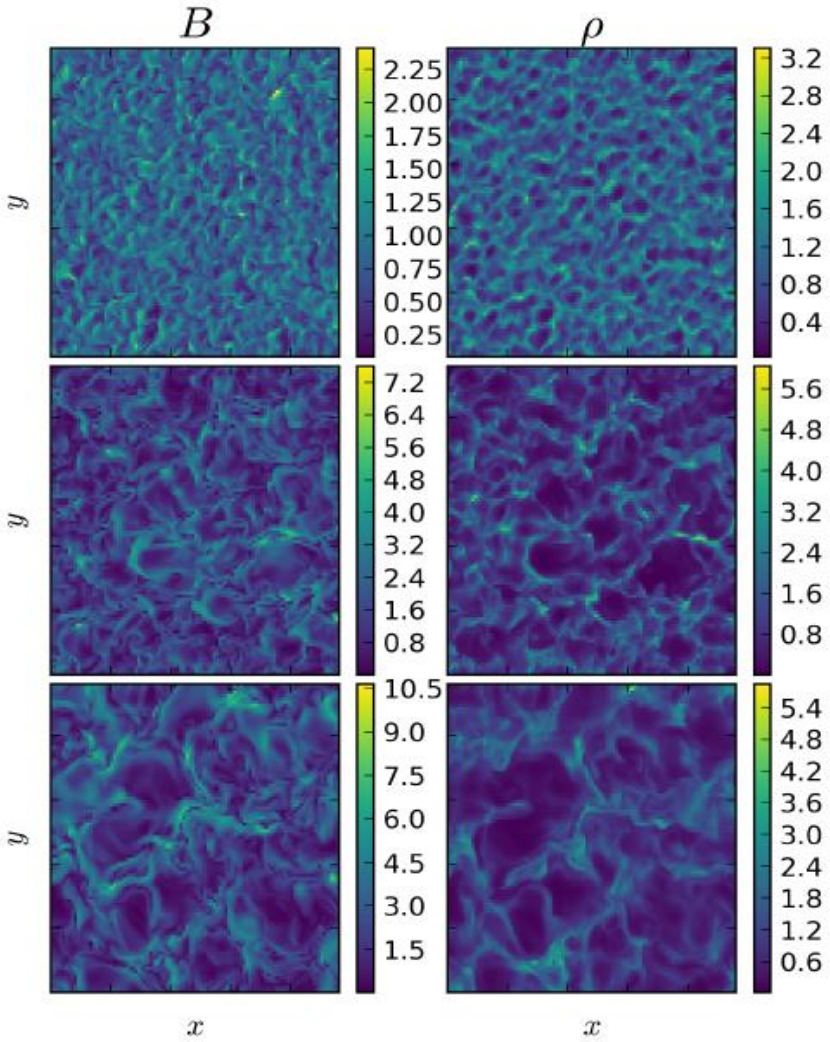

(Matthews et al in preparation)

3D MHD turbulence driven by beam energetic charged particles

Time sequence ⟶

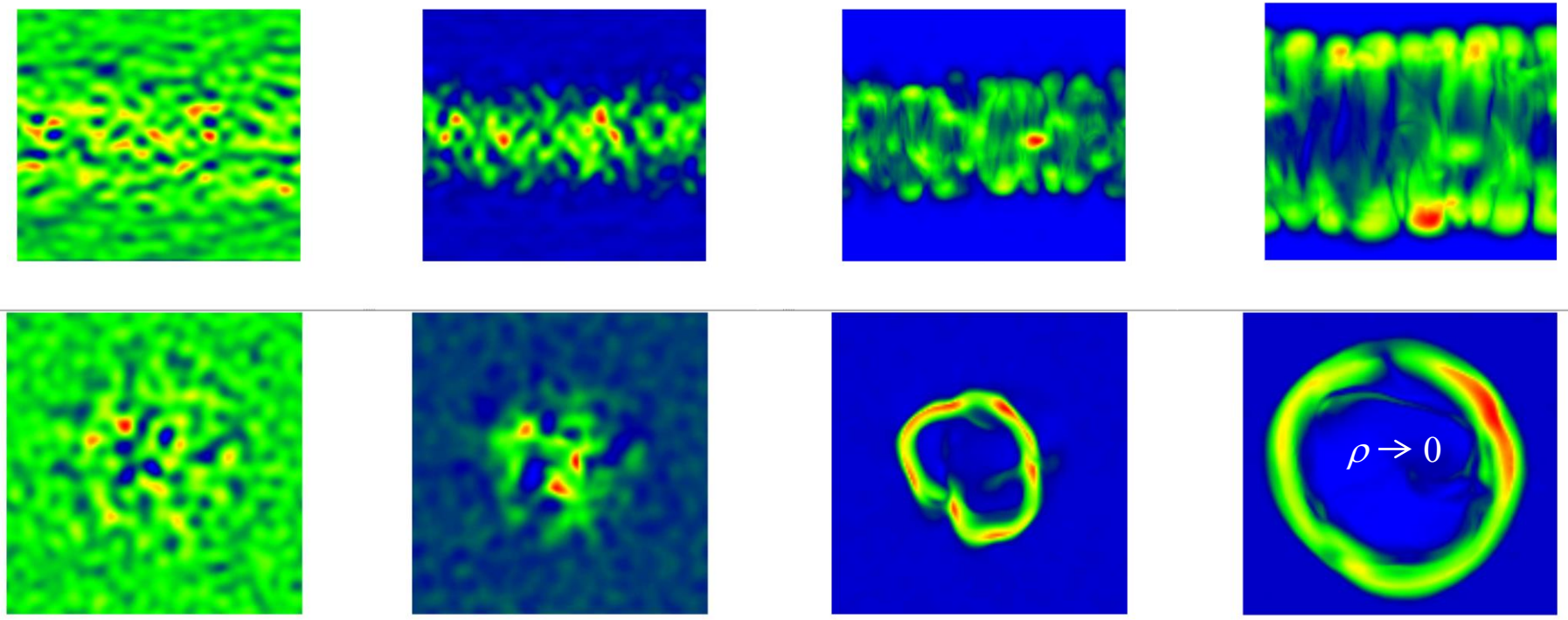

Reason for
Filamentation & self-focussing

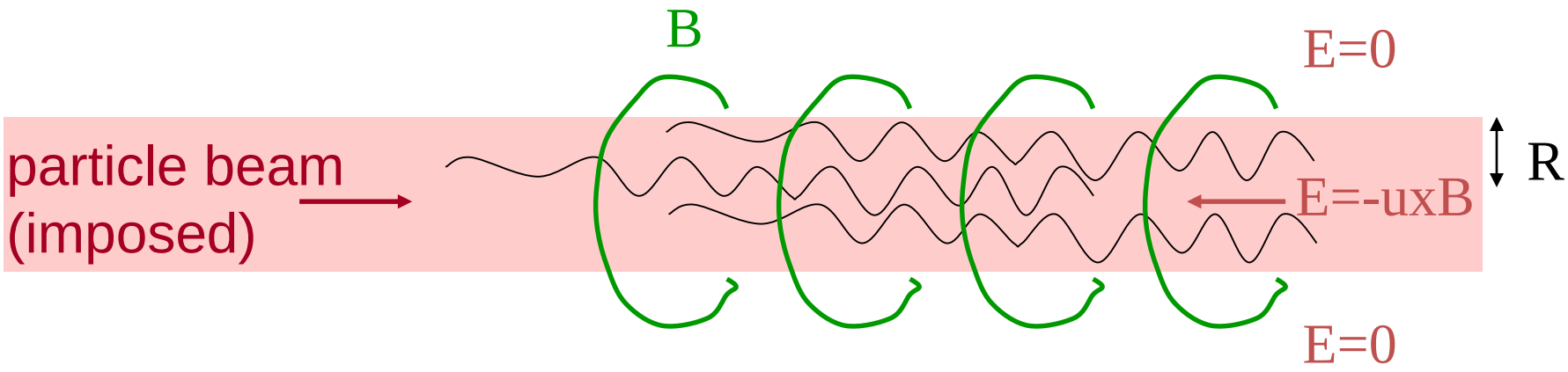

Beam does work generating turbulence

beam energy loss through electric field

curl(E) produces B

focuses particles, evacuates cavity

Beam collimation in laser-plasmas

Do electron beams self-collimate?

Tatarakis et al, PRL 81, 999 (1998)

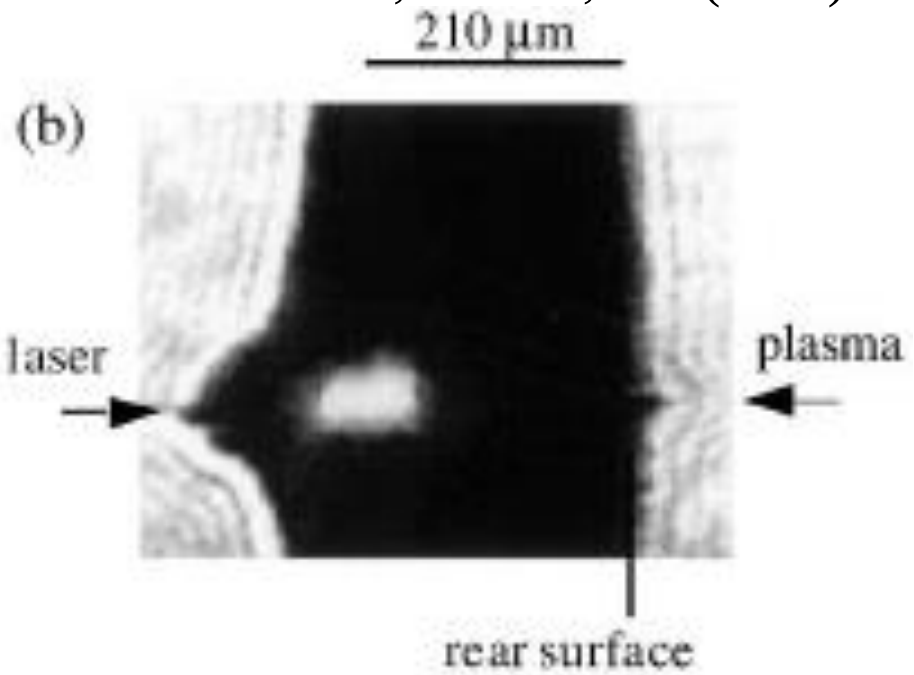

Borghesi et al PRL 83, 4309 (1999)

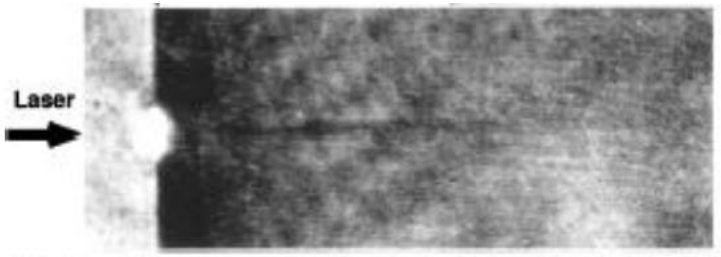

Expts and recent PIC show that Most of the beam energy diverges

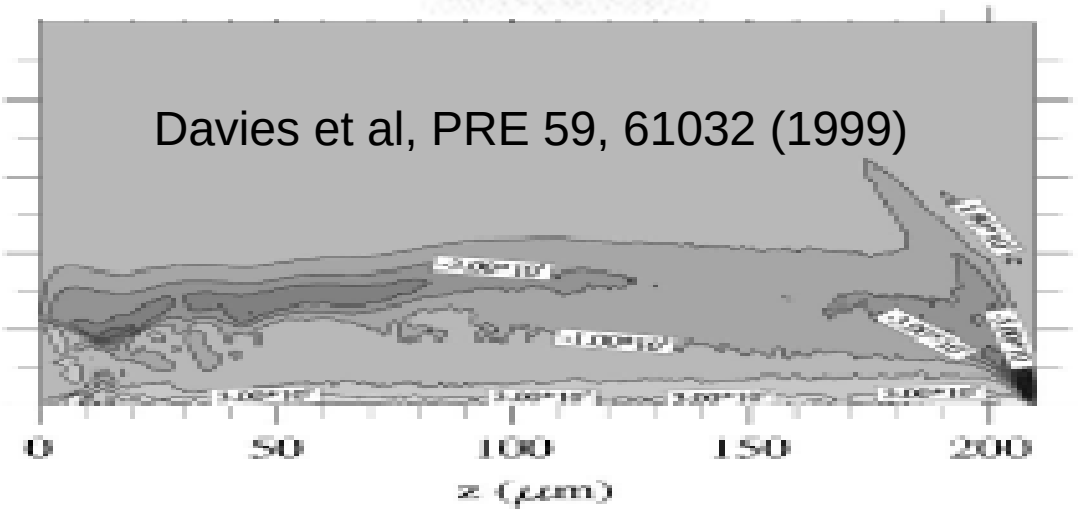

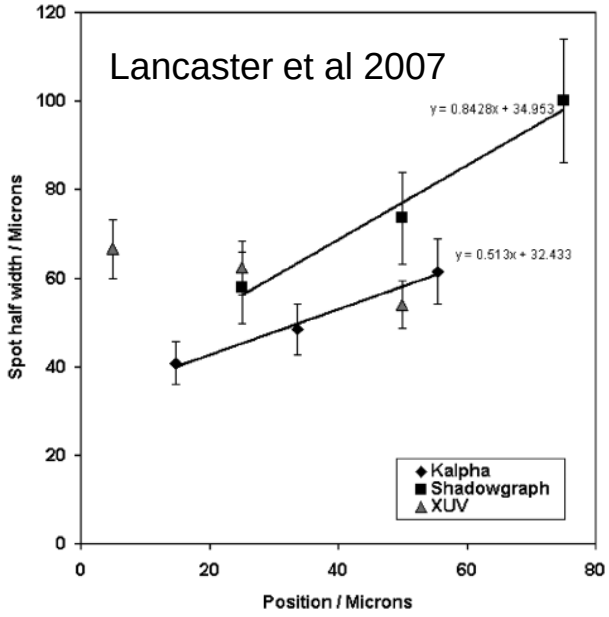

FIG. 3. Plot of K_α, shadowgraphy, and XUV radii vs position.

Resistive generation of magnetic field

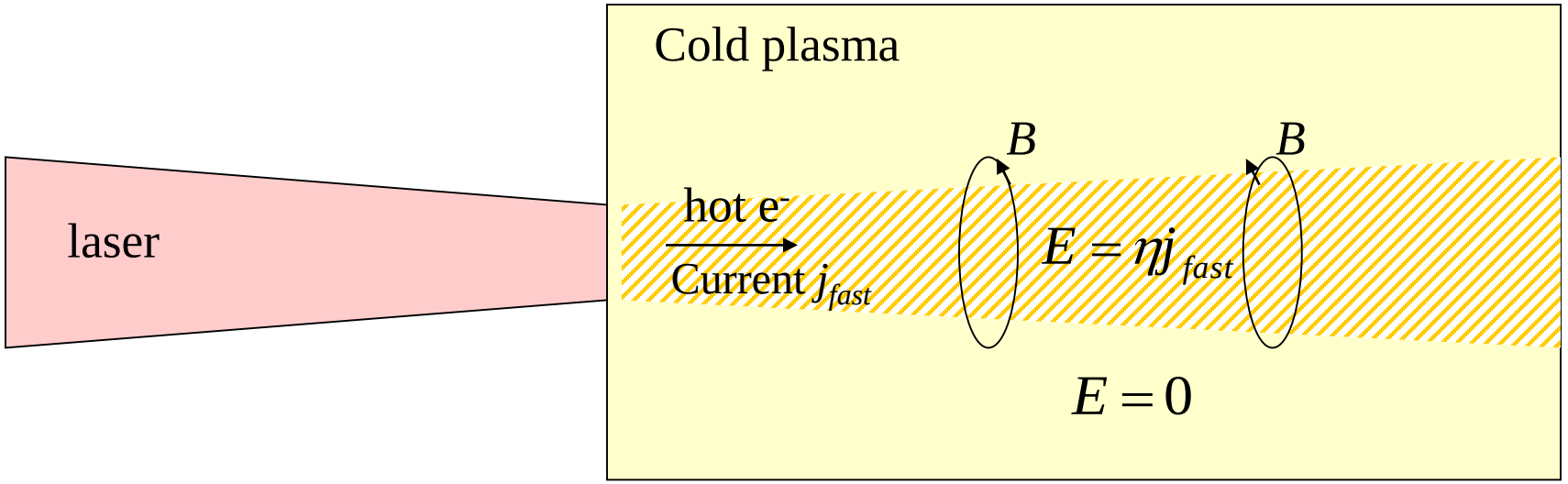

Electric field draws the return current $E = \eta j_{thermal}$ $\frac{\partial B}{\partial t} = -\nabla \times E$

$$\nabla \times B = \mu_0 \left(j_{thermal} + j_{fast} \right)$$

$$\frac{\partial B}{\partial t} = \underbrace{\eta \nabla \times j_{fast} - j_{fast} \times \nabla \eta}_{\text{source}} - \underbrace{\nabla \times \left(\frac{\eta}{\mu_0} \nabla \times B \right)}_{\text{diffusion}}$$

Can we use self-generated magnetic field

in laser-plasmas?

Fast ignition with cones

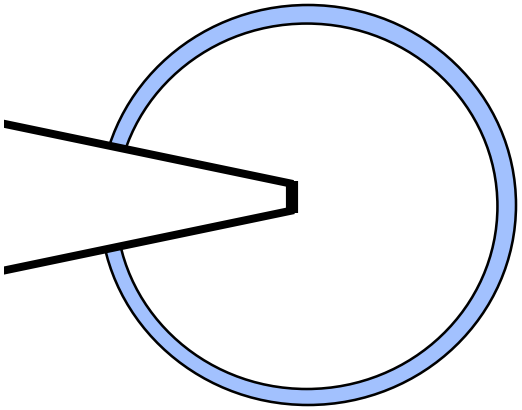

Shell with cone insert

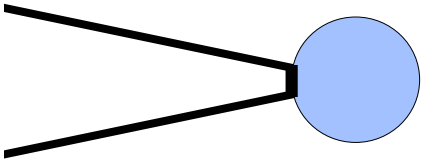

Compress fuel around cone tip

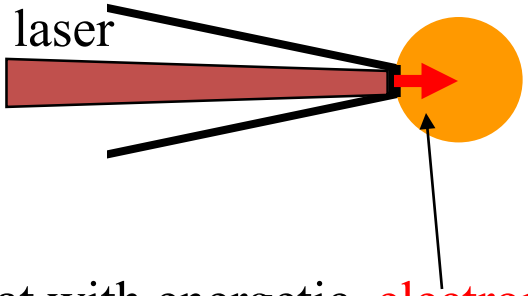

Heat with energetic electrons produced by high intensity laser pulse

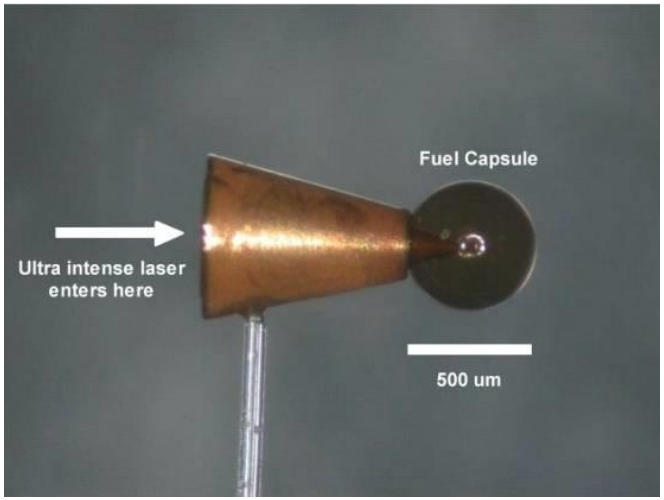

Kodama et al 2001 Nature 412 798

Fast heating of ultrahigh-density plasma as a step towards laser fusion ignition

Kodama et al 2002

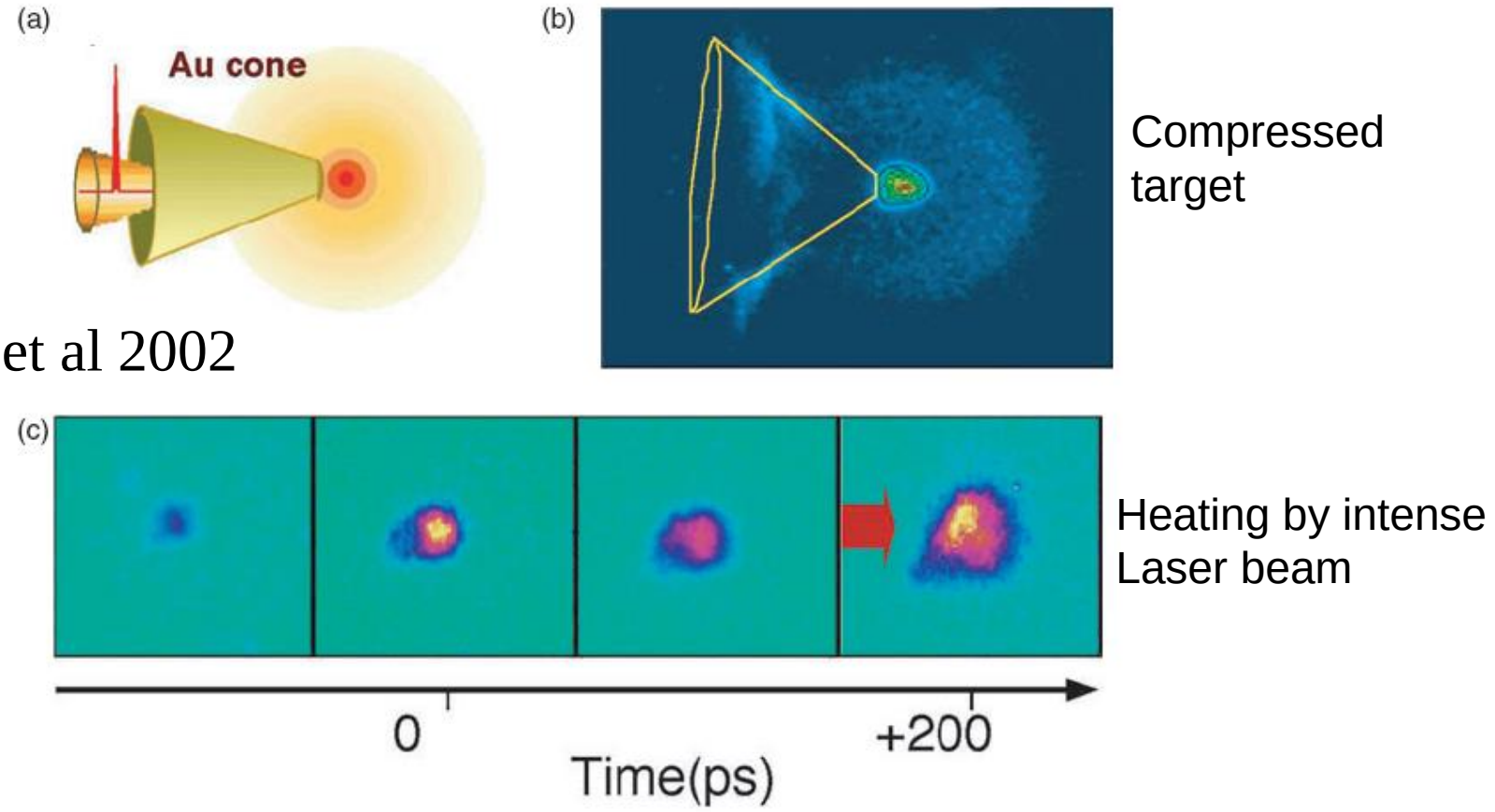

Figure 5. (*a*) External solid-cone guiding. (*b*) X-ray pinhole camera image showing the well imploded core at the tip of the cone. (*c*) X-ray framing images of the core emission for 100 TW laser injection at 150 ps after the peak emission due to the compression.

Beam collimates only if divergence is already small

Condition for collimation

$$(n_{23}^{-0.3} Z^{-0.2} \ln \Lambda^{-0.2} P_{TW}^{0.1} T_{511}^{0.15} R_{\mu m}^{-0.2} t_{p\,\mathrm{sec}}^{-0.2})\,\vartheta < 20 \text{ degrees}$$

(Bell & Kingham 2003)

Reducing the divergence θ:

1) Magnetic field from resistivity gradients

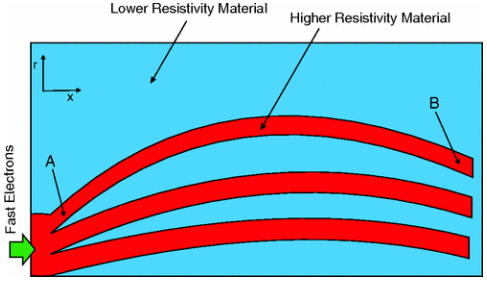

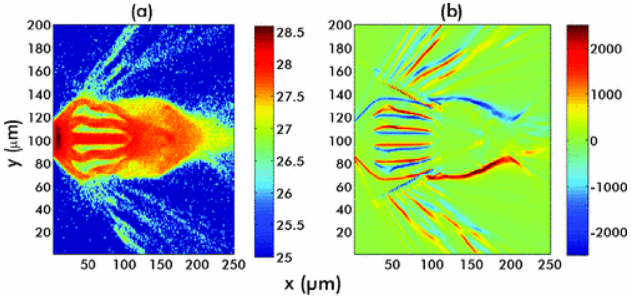

(Robinson et al 2012)

2) Use ions instead of electrons

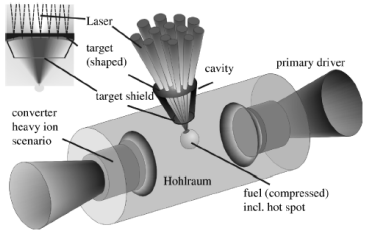

FIG. 1. Indirectly driven fast ignition using a laser accelerated proton beam (not to scale). The rear surface of the laser target is shaped to focus the ion beam into the spark volume.

(Roth et al 2001)

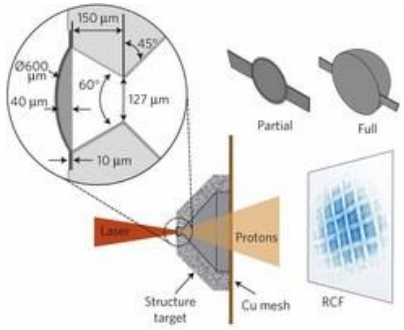

(Bartal et al 2012)

Can charged particle beams drill density cavities?

Provide route to deliver energy to fuel?

Ignition and high gain with ultrapowerful lasers*

Max Tabak,† James Hammer, Michael E. Glinsky, William L. Kruer, Scott C. Wilks, John Woodworth, E. Michael Campbell, and Michael D. Perry
Lawrence Livermore National Laboratory, Livermore, California 94550

Rodney J. Mason
Los Alamos National Laboratory, Los Alamos, New Mexico 87545

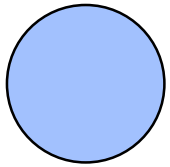

Cold compressed fuel

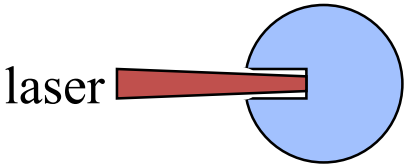

Drill hole with laser

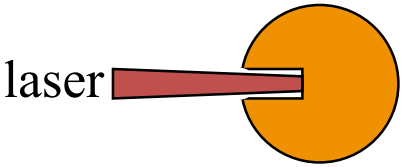

Heat with very high power laser

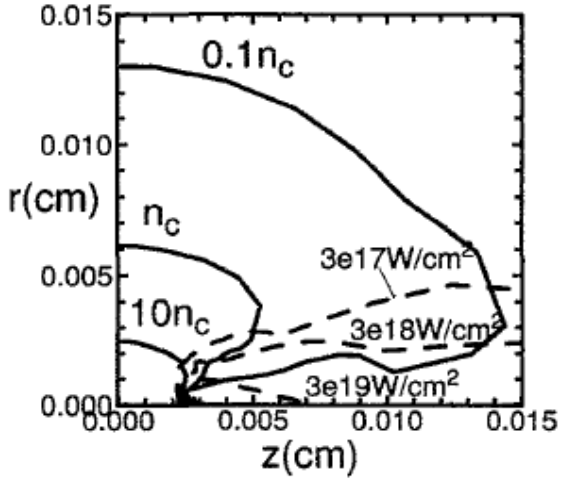

FIG. 9. Isocontours of laser intensity and electron density (multiples of critical density) 21 ps after the start of the hole-boring calculation.

Create cavity with current of energetic ions?

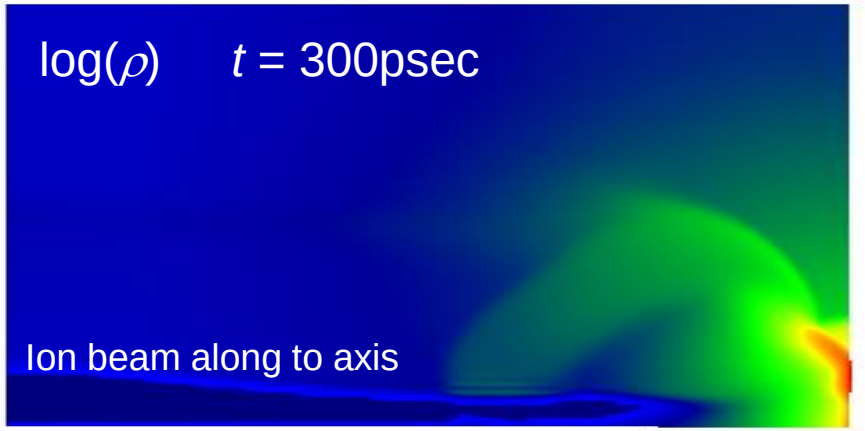

As in astrophysics:

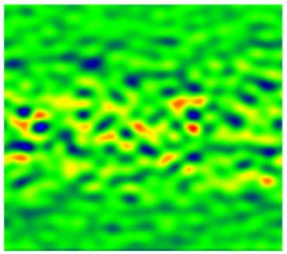
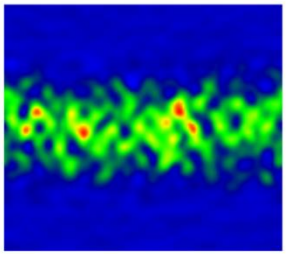
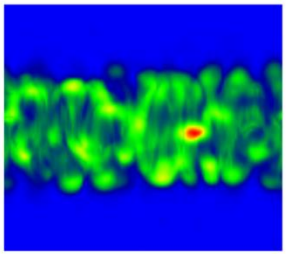
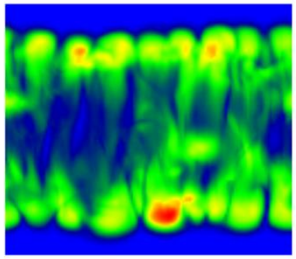
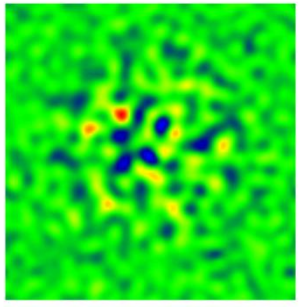
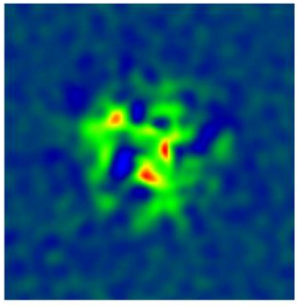
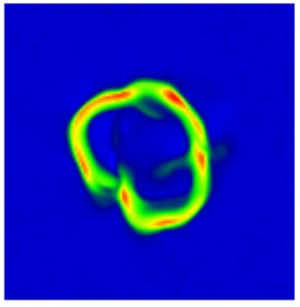
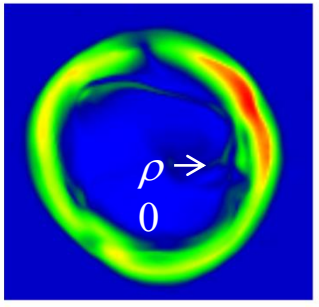

Hydro cavity driven by ions through $j_{beam} \times B$

Target initially
100 gm cm^{-3} inside125μm radius,
r^{-2} outside 125μm
500eV (ideal gas)

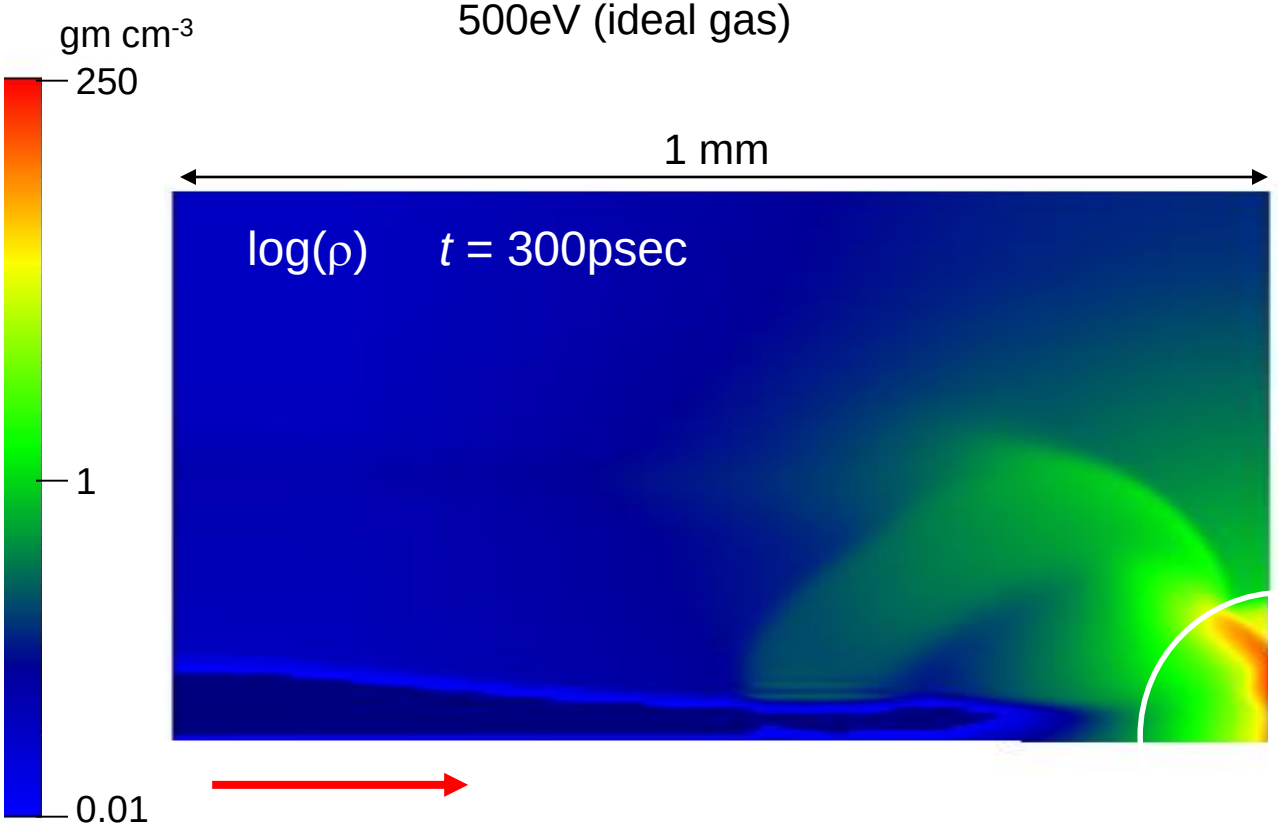

Initially

$\rho = 100\ (r/125\mu m)^{-2}$ gm cm^{-3}

125μm

$\rho = 100$ gm cm^{-3}

Ion beam on axis (straight line propagation)

500keV protons Beam radius 30μm

Power 140 TW Intensity 5x10^{18} W cm^{-2} Beam energy 42kJ

Shock ignition

Another way to heat the fuel

The role of energetic particle transport

Advanced ignition

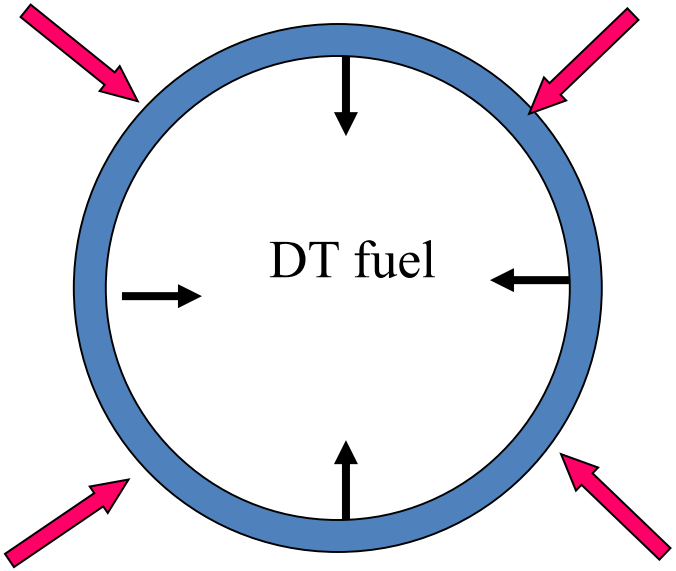

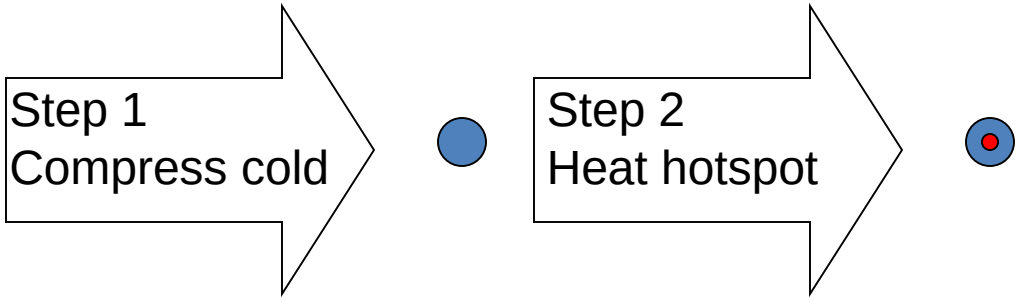

Potentially:
Reduce laser from MJ to ~100kJ
Smaller IFAR, lower implosion velocity, less instability

Heating variants:

Fast ignition: heat with ~MeV electrons generated by very intense laser

Shock ignition: heat with converging shock driven by intense laser

Proton (ion) drive: heat with ion beam produced by very intense laser

Shock ignition

- Compress target on low isentrope
- Final laser spike launches ignition shock

Figures from: Betti et al (2008) JPhys conf series 112 022024

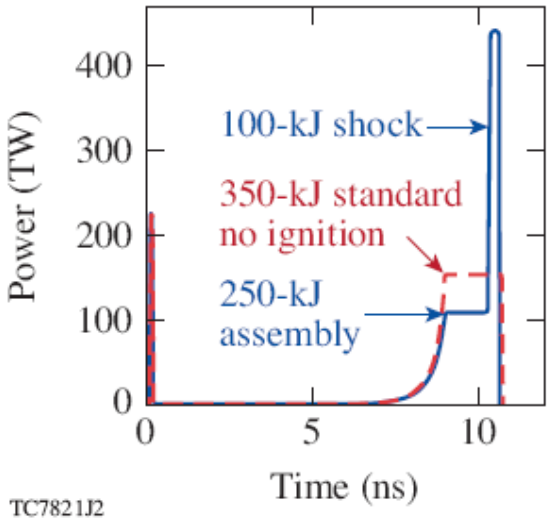

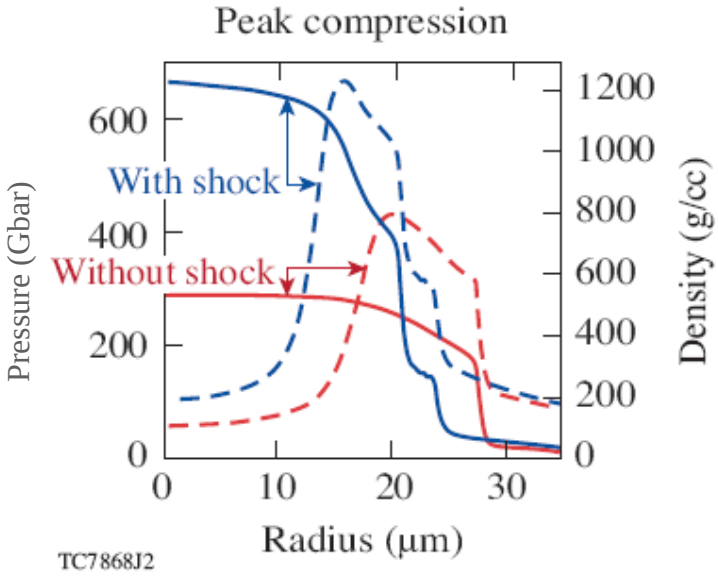

Issue: Is high intensity laser pulse reflected by Raman, Brillouin etc?
High energy (100keV) electrons actually an advantage

Attractive feature: may be possible with polar drive as in NIF
Symmetry from hydrodynamics and thermal conduction

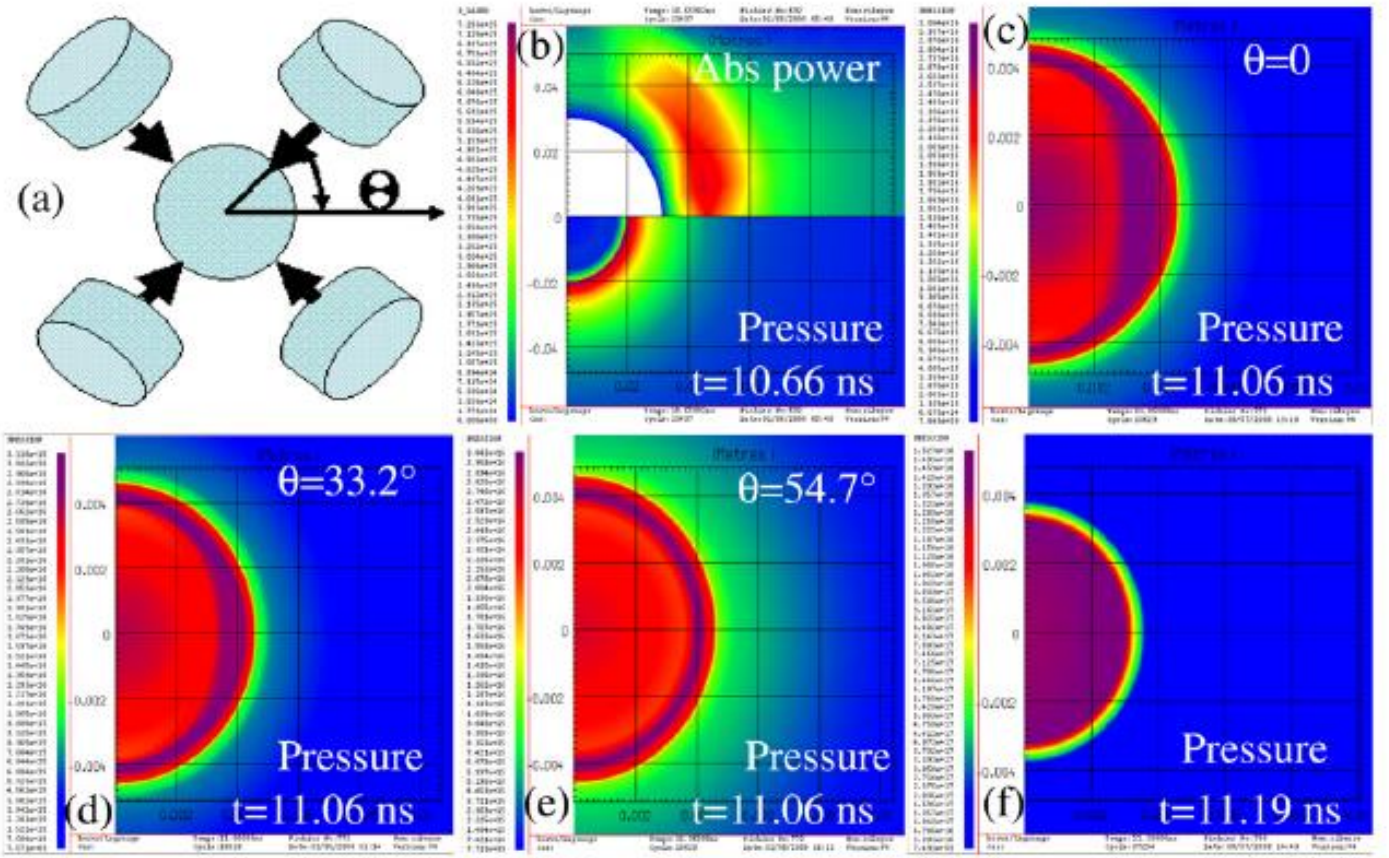

Figure 10. (*a*) The ignition beams are disposed along two symmetric cones of half-angle θ. (*b*) Simulated laser absorbed power and plasma pressure during the spike for $\theta = 0$. (*c*) Pressure distribution inside the shell 400 ps after shock launch for $\theta = 0$. (*d*) The same as (*c*) for $\theta = 33.2°$. (*e*) The same as (*c*) for $\theta = 54.7°$. (*f*) The distribution of pressure inside the shell 530 ps after the launch time is the same for the three considered angles.

Vlasov-Fokker-Planck (VFP) simulation

The VFP regime

Ablating laser plasmas: $L \approx \lambda \sqrt{\frac{m_i}{m_e}}$

Astro particle acceleration: $L = \frac{1}{3}\frac{c}{u}\lambda$

Requires: $\underbrace{\frac{\partial f}{\partial t} + \mathbf{v}.\frac{\partial f}{\partial \mathbf{r}} - e(\mathbf{E} + \mathbf{v}\times\mathbf{B}).\frac{\partial f}{\partial \mathbf{p}}}_{\text{Vlasov equation (collisioness)}} = \underbrace{C(f)}_{\text{Collisions Fokker-Planck}}$

Particle-in-cell (PIC) codes best for collisionless plasmas

PIC difficult when:

- Collisions are important
- Or, small number of energetic particles interacting with background plasma
- Or, plasma is nearly thermalised

Vlasov equation (no collisions)

Vlasov code solves for *f* in (**r,p**) space

$$\frac{\partial f}{\partial t} + \mathbf{v}.\frac{\partial f}{\partial \mathbf{r}} - e\left(\mathbf{E} + \mathbf{v}\times\mathbf{B}\right).\frac{\partial f}{\partial \mathbf{p}} = 0$$

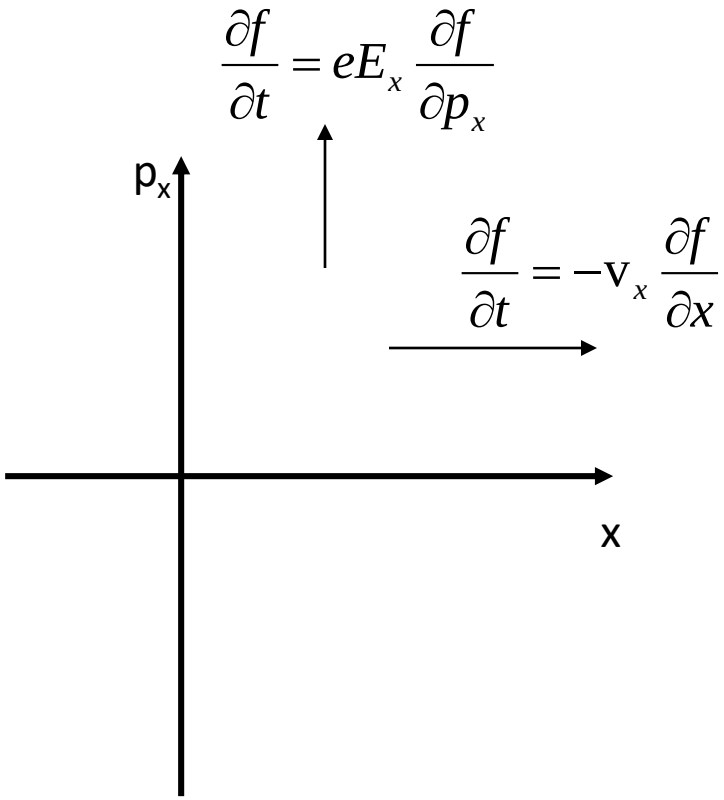

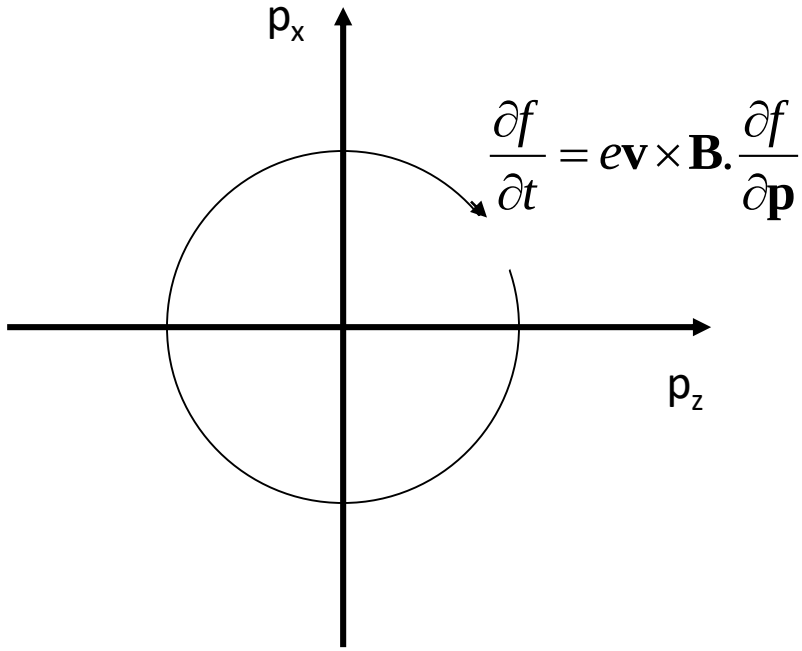

In (x,p_x,p_z) natural to use square grid
but magnetic field gives diagonal motion

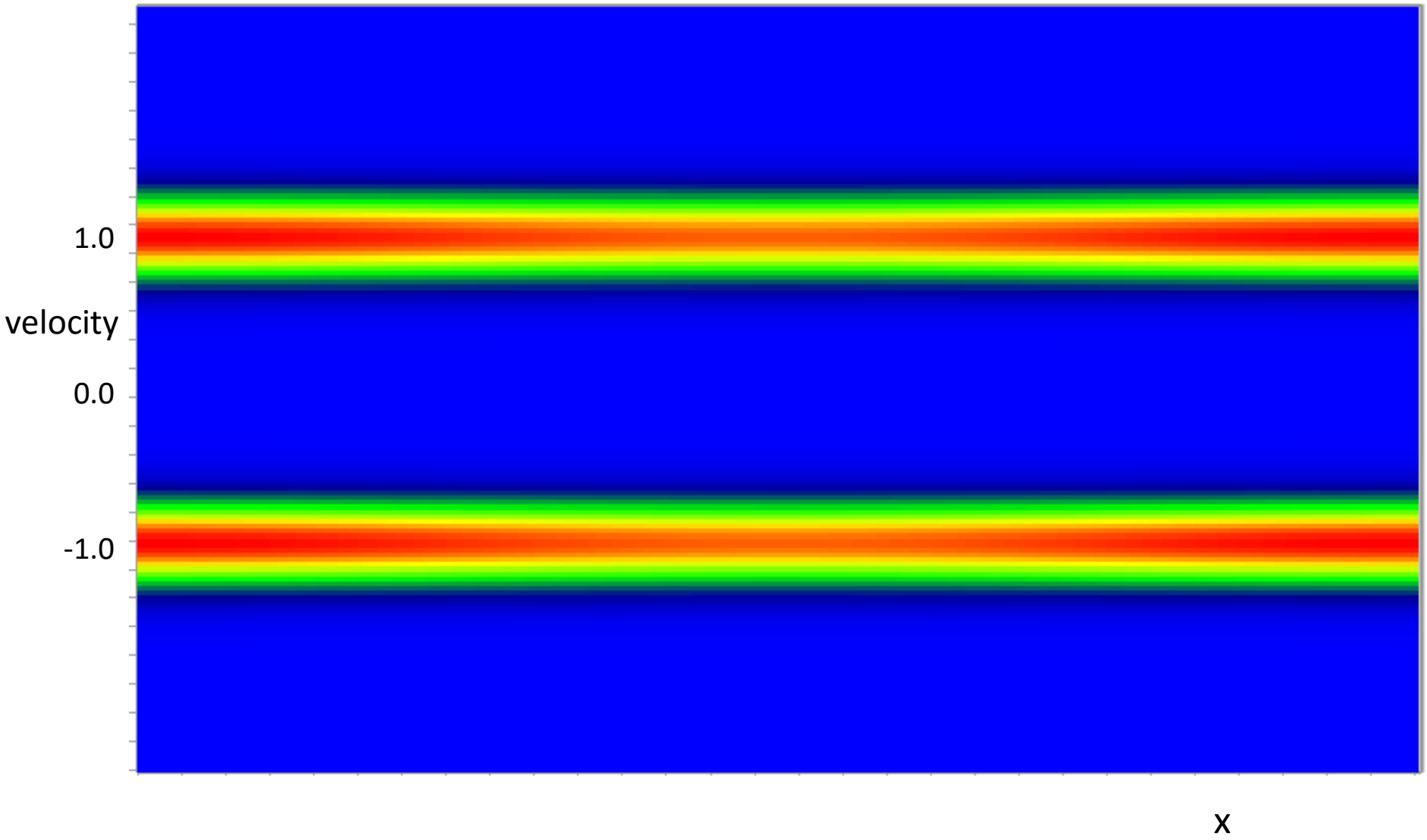
1.0
velocity
0.0
-1.0
x

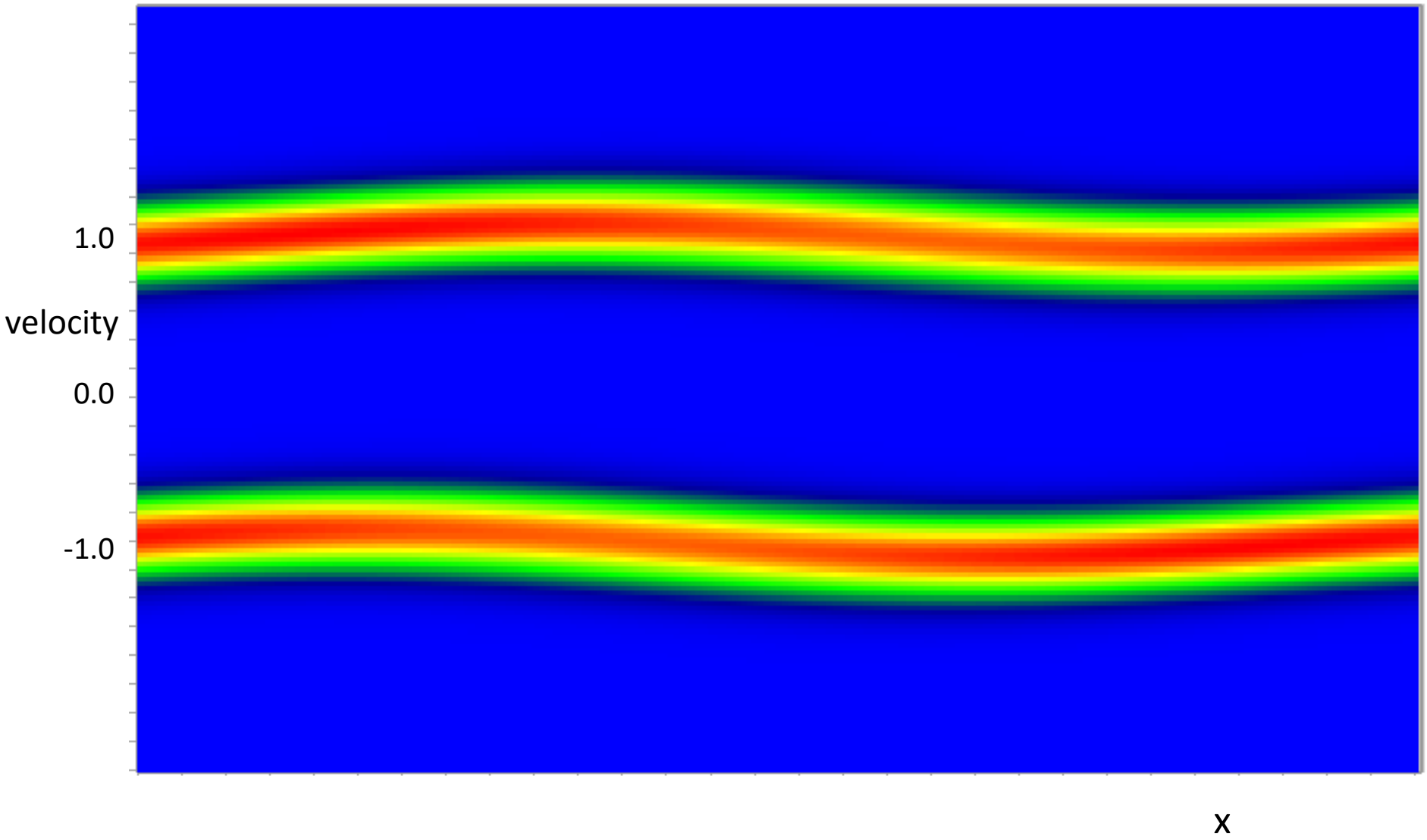
1.0
velocity
0.0
-1.0
x

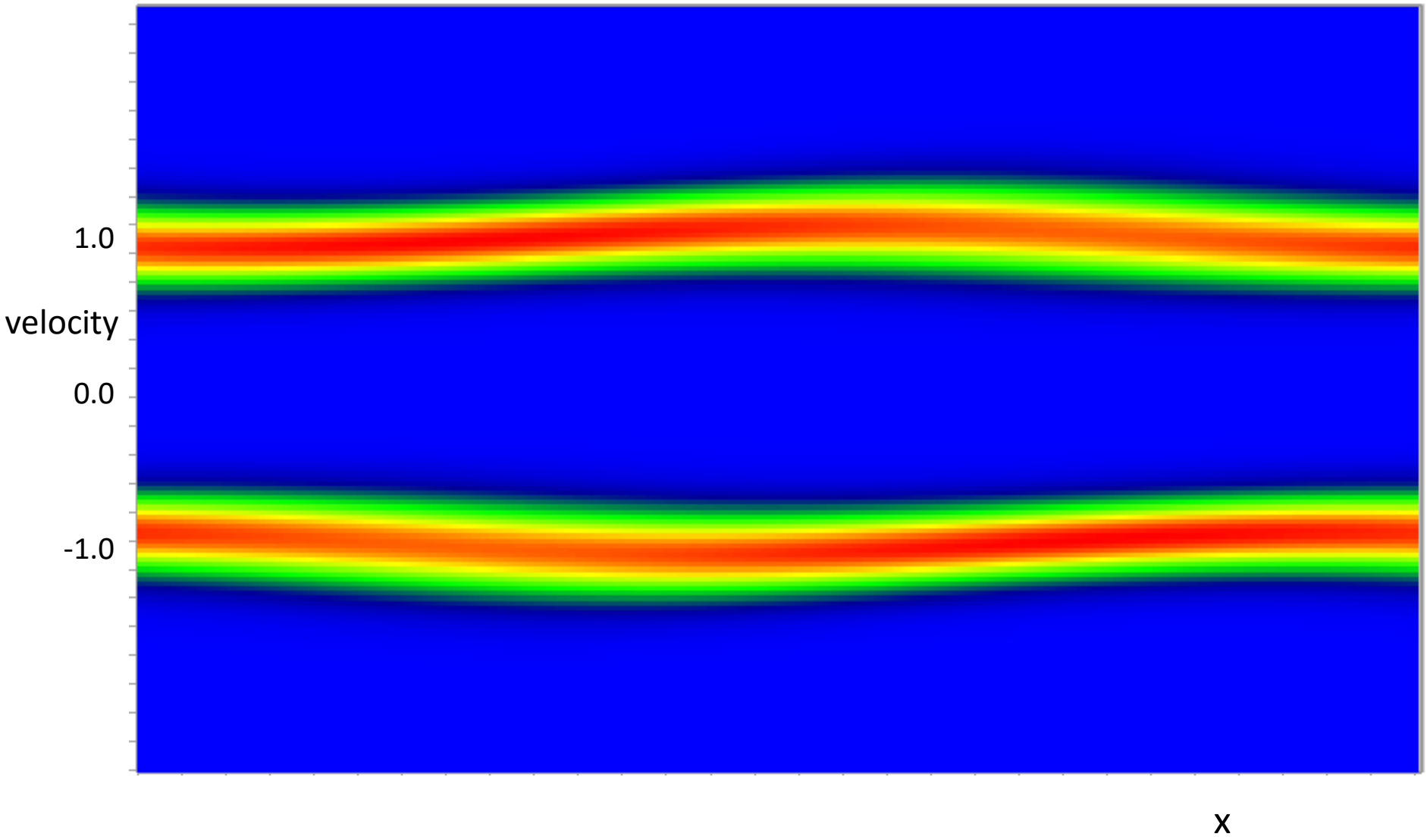
1.0
velocity
0.0
-1.0
x

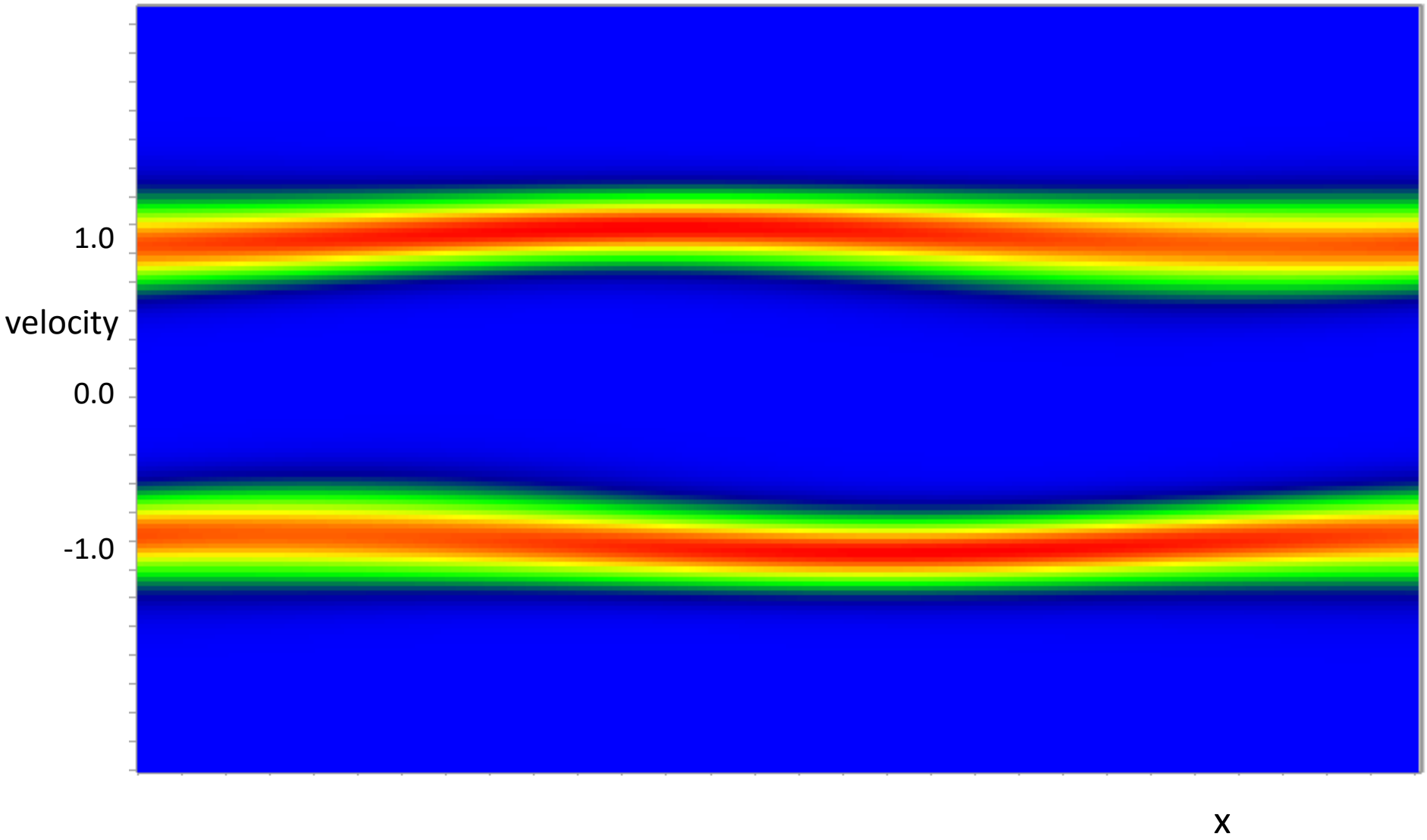
1.0
velocity
0.0
-1.0
x

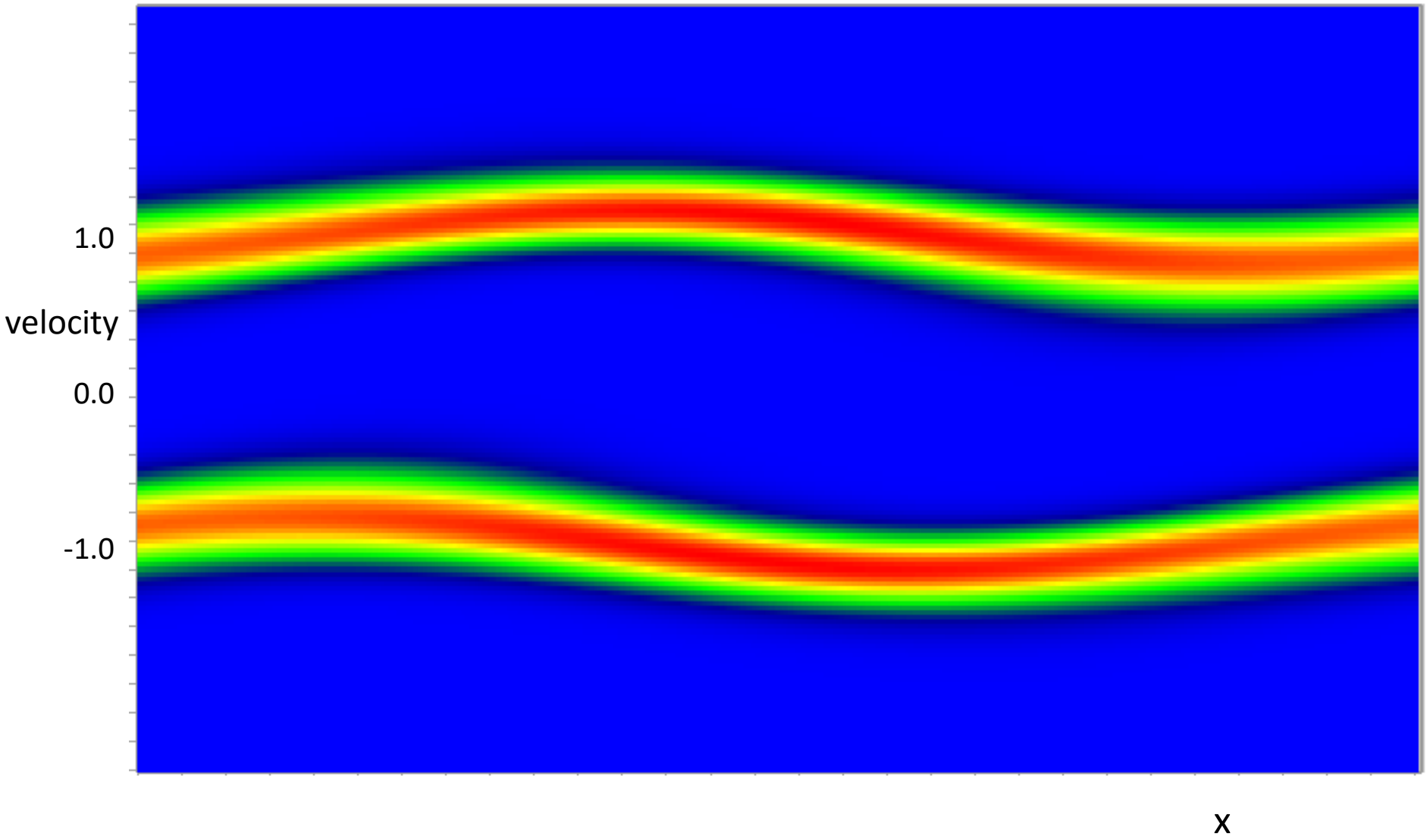
1.0
velocity
0.0
-1.0
x

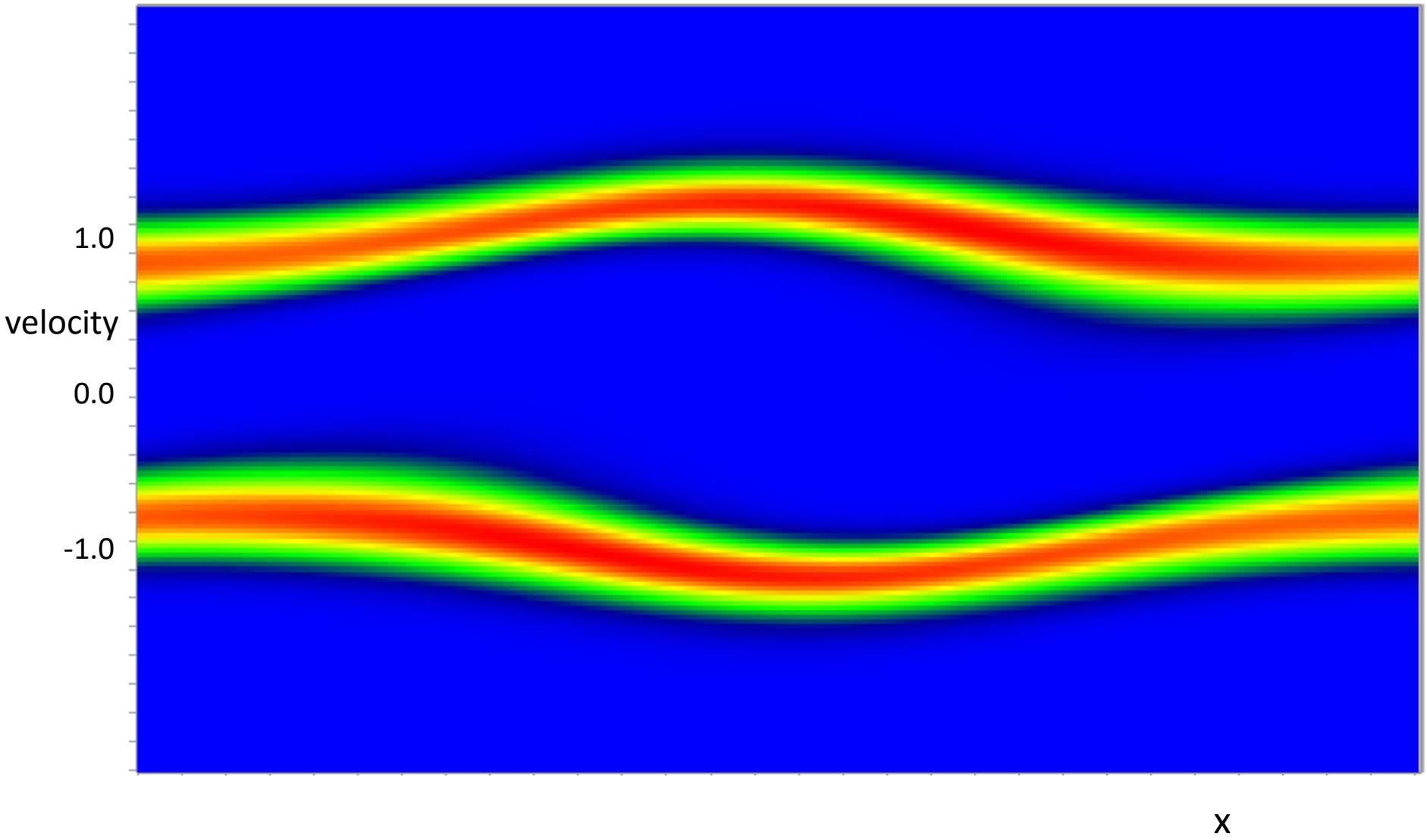
1.0
velocity
0.0
-1.0
x

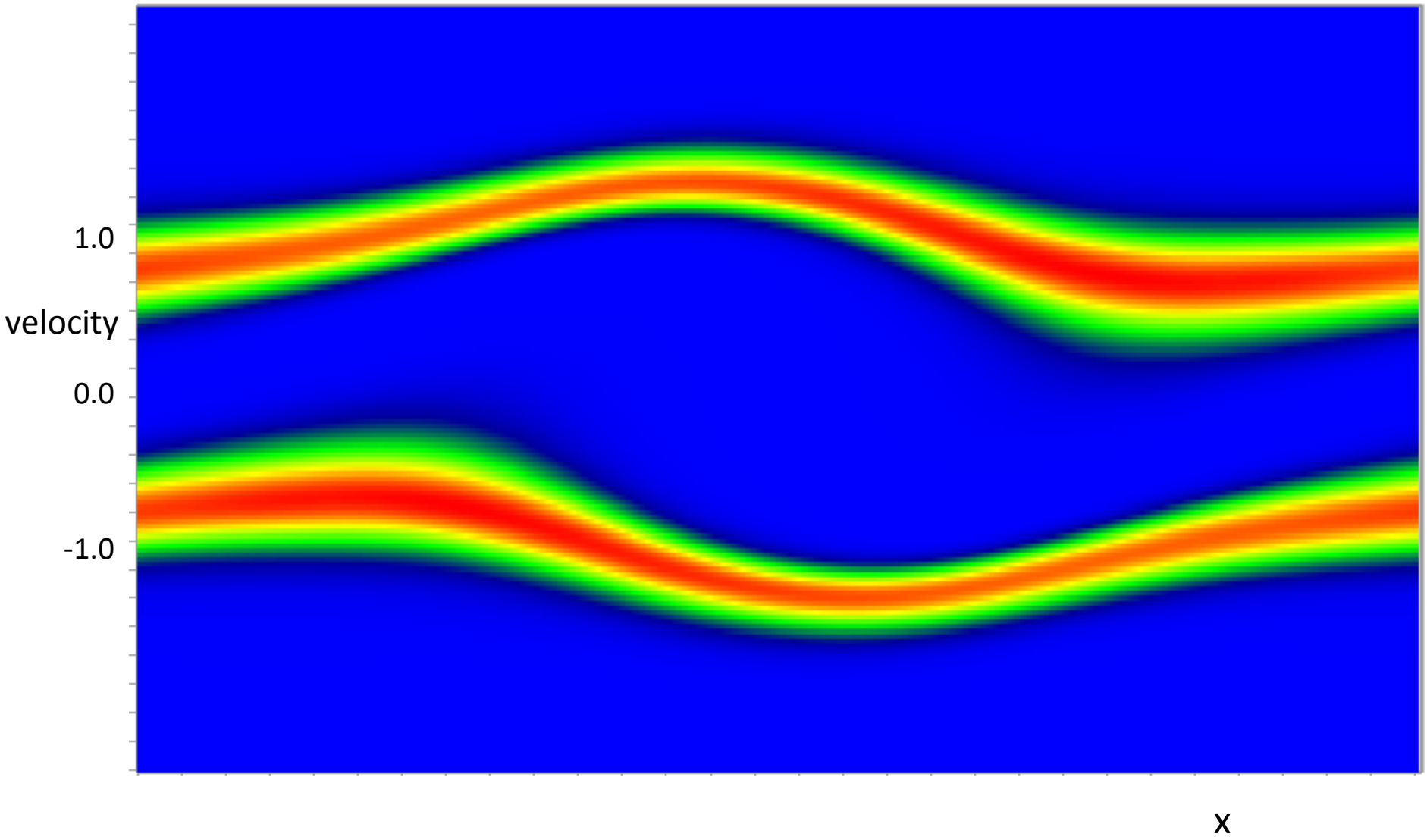
1.0
velocity
0.0
-1.0
x

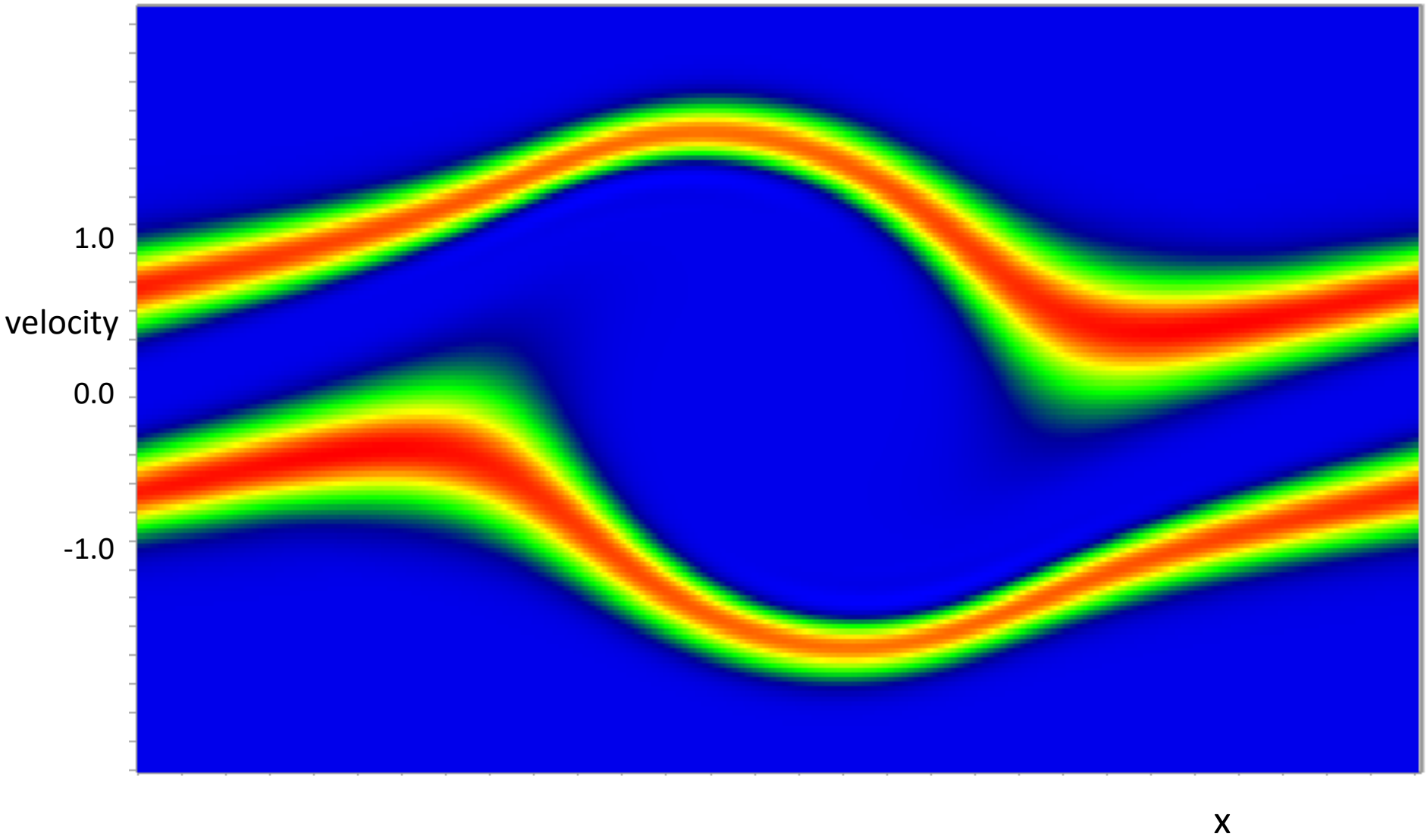
1.0
velocity
0.0
-1.0
x

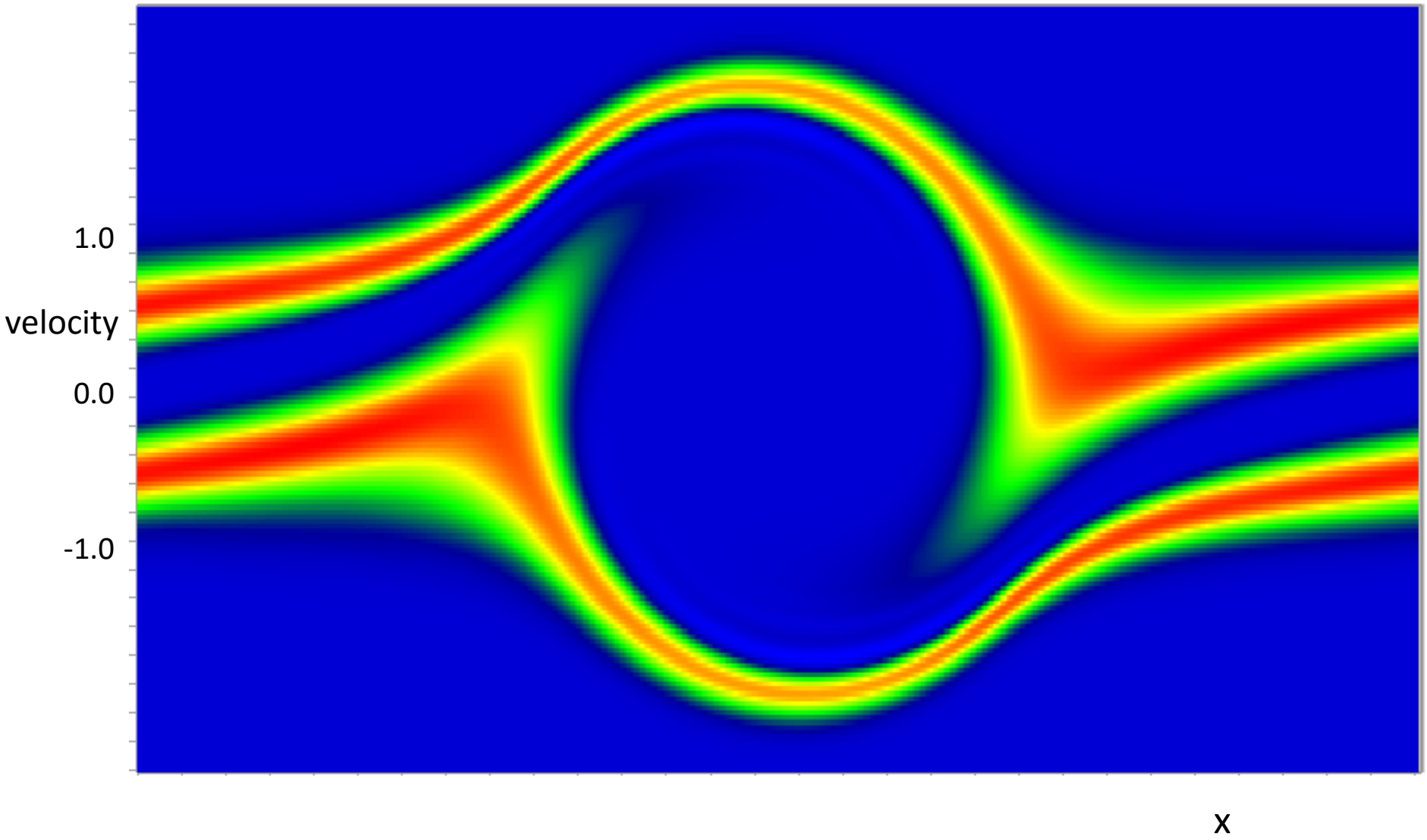
1.0
velocity
0.0
-1.0
x

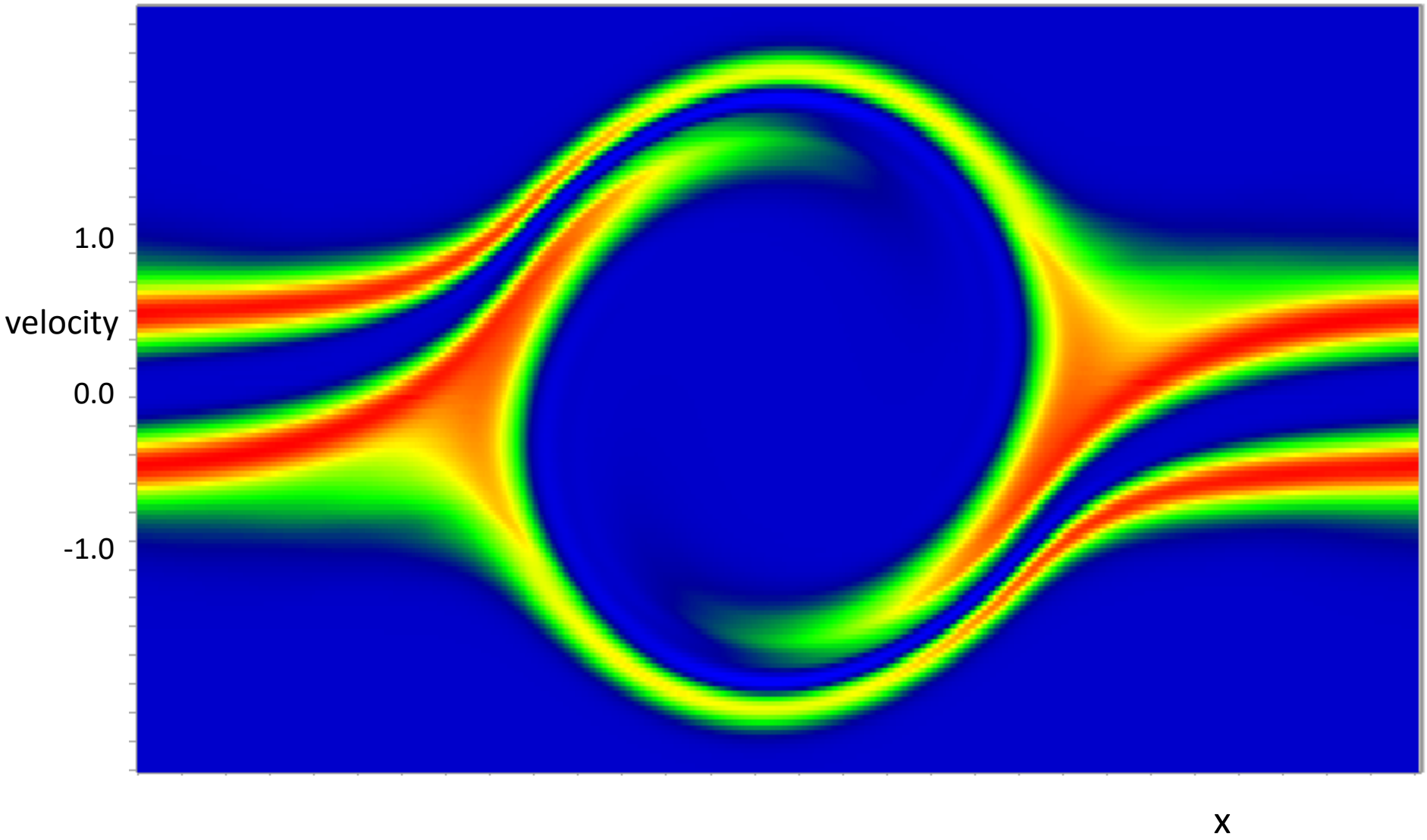
1.0
velocity
0.0
-1.0
x

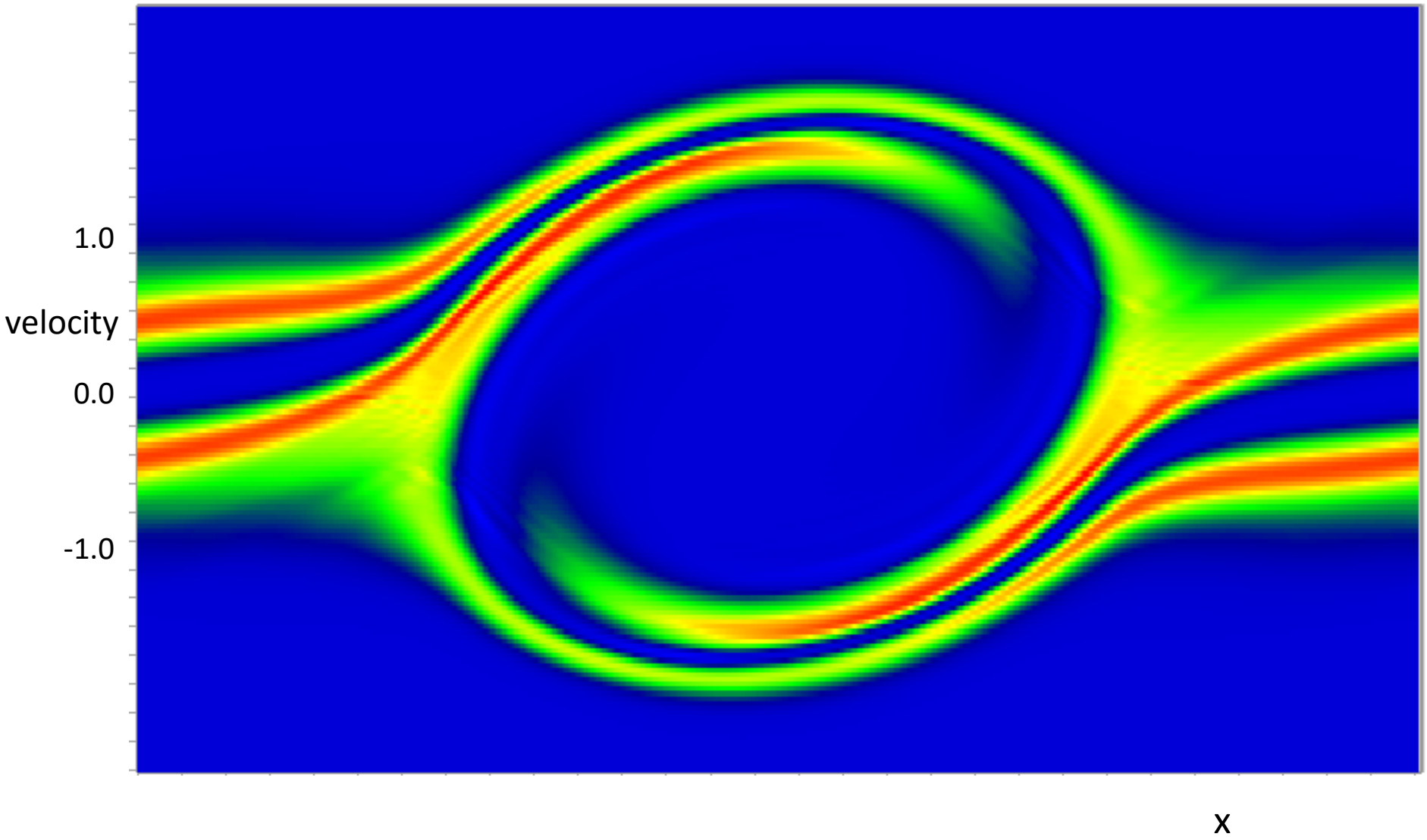
1.0
velocity
0.0
-1.0
x

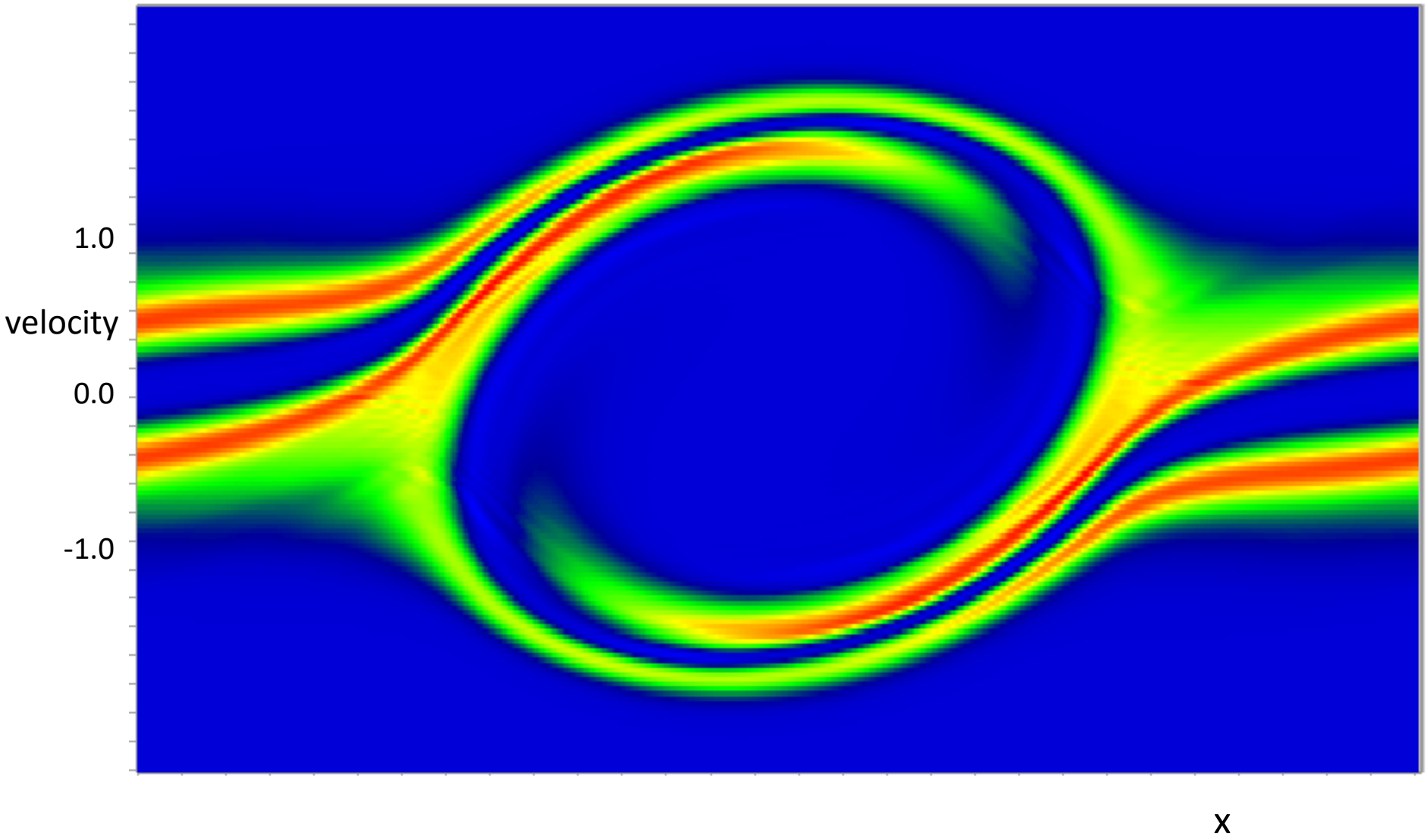
1.0
velocity
0.0
-1.0
x

Fokker-Planck equation for collisions

Small angle scattering: diffusion & advection in momentum space

$$C(f) = \frac{\partial}{\partial \mathbf{p}} . \left(\underset{\approx}{\mathbf{D}} . \frac{\partial f}{\partial \mathbf{p}} - \mathbf{A} f \right)$$

Diffusion tensor

Advection in momentum space
eg slowing down

Diffusion + advection = ‘Fokker-Planck’ equation

The Vlasov-Fokker-Planck (VFP) equation

$$\underbrace{\frac{\partial f}{\partial t} + \mathbf{v}.\frac{\partial f}{\partial \mathbf{r}} - e\left(\mathbf{E} + \mathbf{v}\times\mathbf{B}\right).\frac{\partial f}{\partial \mathbf{p}}}_{\text{Vlasov equation (collisioness)}} = \underbrace{C(f)}_{\text{Collisions Fokker-Planck}}$$

$f(x, y, z, p_x, p_y, p_z, t)\, dx\, dy\, dz\, dp_x\, dp_y\, dp_z$

= number of electrons in phase space volume $dx\, dy\, dz\, dp_x\, dp_y\, dp_z$

Natural expansion for *f*

$$f = \sum_{n=0}^{n_{\max}} \sum_{m=-n}^{n} f_n^{\,m}(r, z, p) P_n^{|m|}(\cos\vartheta) e^{im\varphi}$$

Spherical harmonics

In 1D need only m=0 harmonics – Legendre polynomials

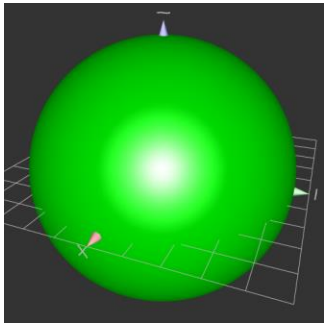

l=0

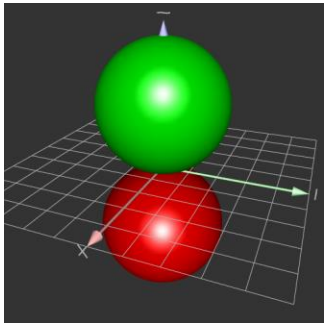

l=1

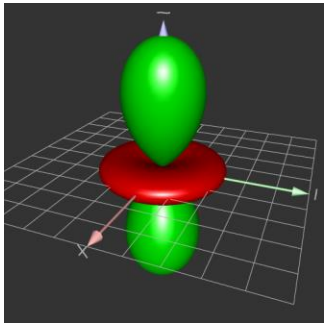

l=2

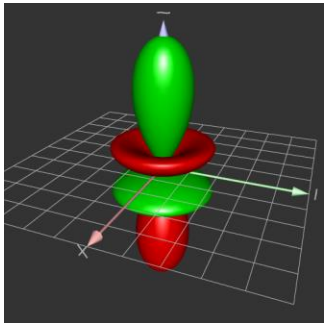

l=3

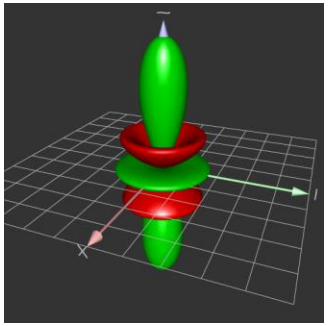

l=4

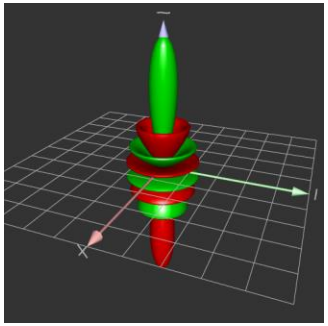

l=7

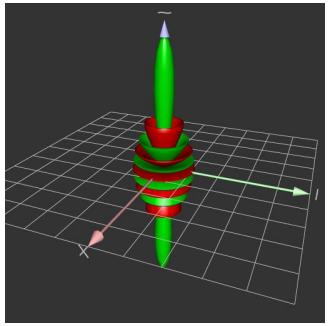

l=10

people.csail.mit.edu/sparis/sh/index.php?img=64

l=10 harmonics, m=0, 5, 10

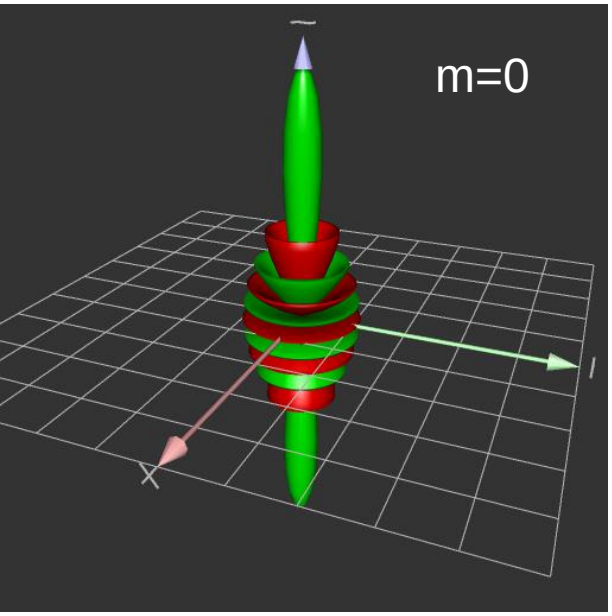

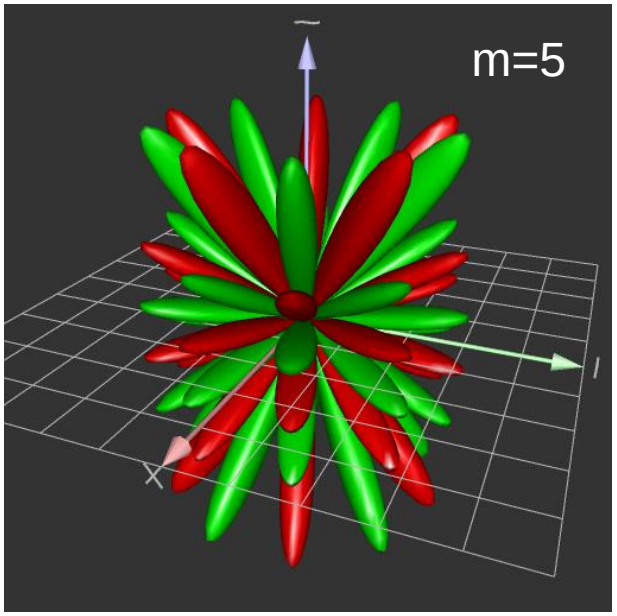

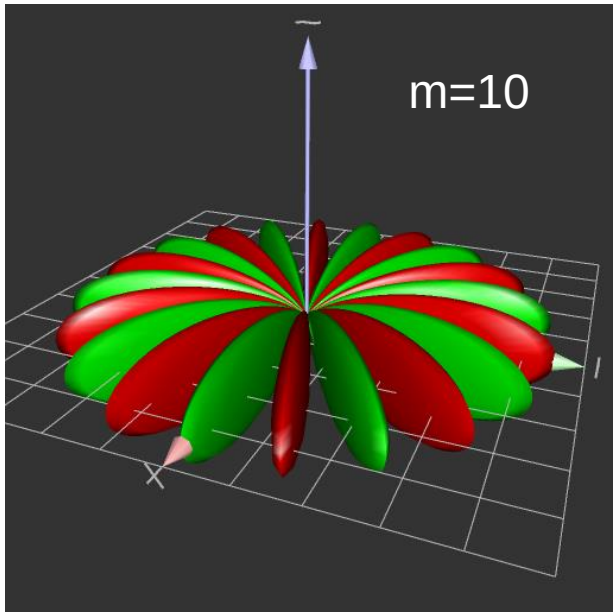

people.csail.mit.edu/sparis/sh/index.php?img=64

Magnetic field

Magnetic field rotates in momentum

For example: ‘Vertical’ B rotates l=10, m=0

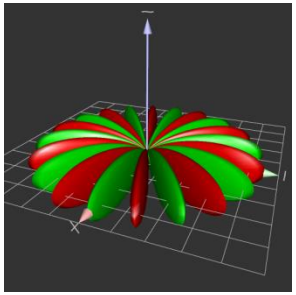

Algebraic: no differentials

$eB/m_e = 2 \times 10^{13} sec^{-1}$ when B=1MG

Collision scattering in spherical polars

$$\frac{\partial f}{\partial t} = \frac{1}{p^2}\frac{\partial}{\partial p}\left(p^2 D_p \frac{\partial f}{\partial p} - Af \right) + \frac{1}{p^2 \sin\vartheta}\frac{\partial}{\partial \vartheta}\left(\sin\vartheta\, D_\perp \frac{\partial f}{\partial \vartheta} \right) + \frac{D_\perp}{p^2 \sin^2\vartheta}\frac{\partial^2 f}{\partial \phi^2}$$

Angular scattering stronger than energy diffusion $D_\perp \approx ZD_p$

Simplifies to $\frac{\partial f_l^m}{\partial t} = \frac{1}{p^2}\frac{\partial}{\partial p}\left(p^2 D_p \frac{\partial f_l^m}{\partial p} - A f_l^m \right) - \frac{l(l+1)}{2}\frac{D_\perp}{p^2} f_l^m$

Dominant term

Angular scattering $\frac{\partial f_l^m}{\partial t} = -\frac{l(l+1)}{2}\frac{D_\perp}{p^2} f_l^m$ has solution $f_l^m \propto \exp\left(-\frac{l(l+1)}{2}\frac{D_\perp}{p^2} t \right)$

High order harmonics decay rapidly – can truncate harmonic expansion

VFP codes in spherical harmonics:

Easy for collisions

Memory requirement low compared with square grid Vlasov

The challenge for non-collisional high anisotropy
(making progress – eg 2-stream instability)

1D ablation profiles

laser

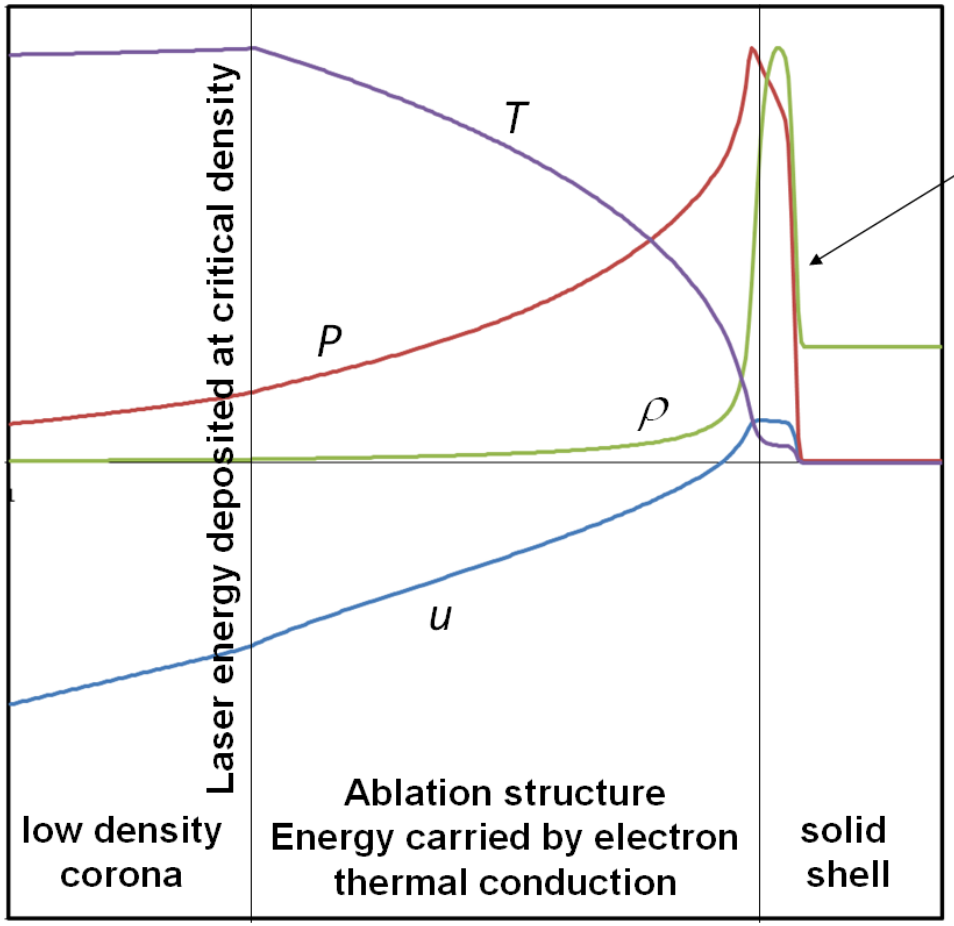

$$L \approx \lambda \sqrt{\frac{m_i}{m_e}}$$ ~ 60 electron mean free paths

Non-local heat transport

Shock ignition

P_{max}=640Mbar at edge of high density

t = 32 psec

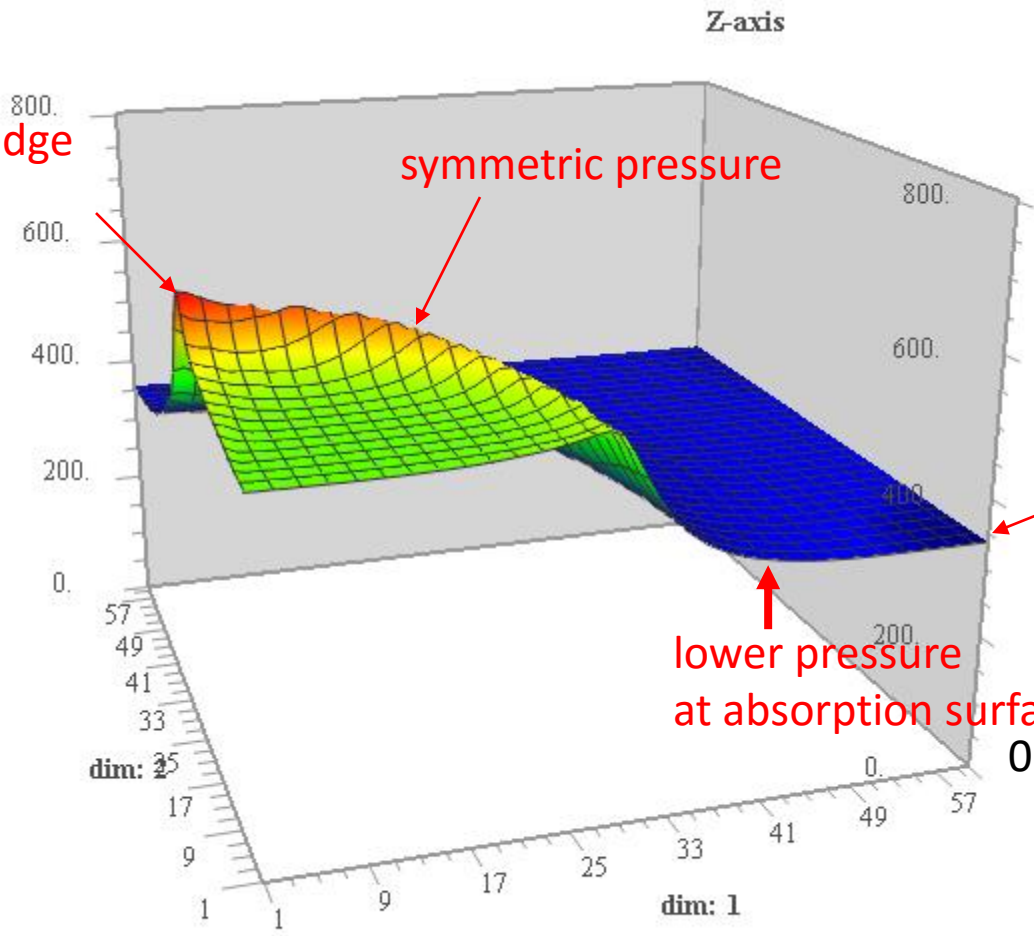

Polar drive, absorbed intensity = $8 \times 10^{16} \cos^2\theta$ Wcm^{-2}

Absorption at $n = 10^{22}$ cm^{-3}

Constant for 32psec

T_{hot}=100keV

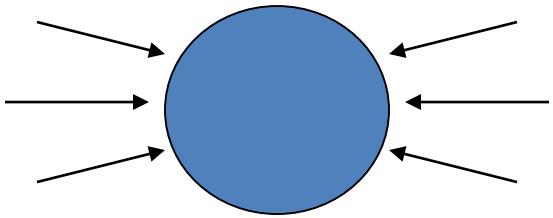

Shock ignition

$I_{absorbed} = 8 \times 10^{15} \cos^2\theta$ Wcm^{-2}, T_{hot}=10keV, t=28psec

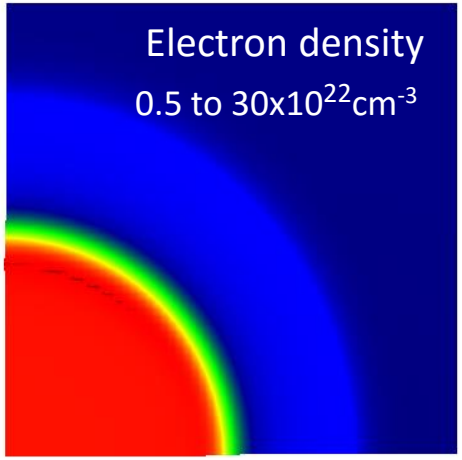

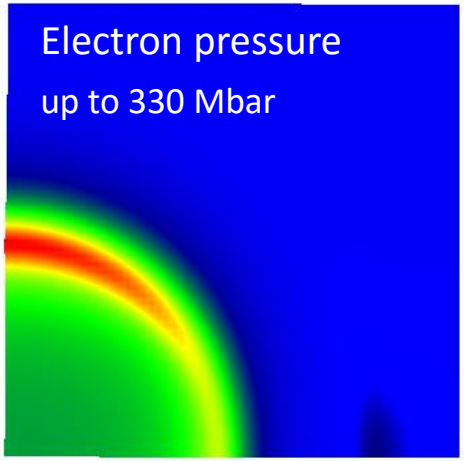

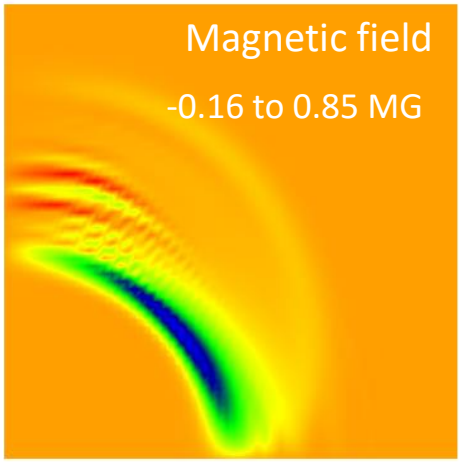

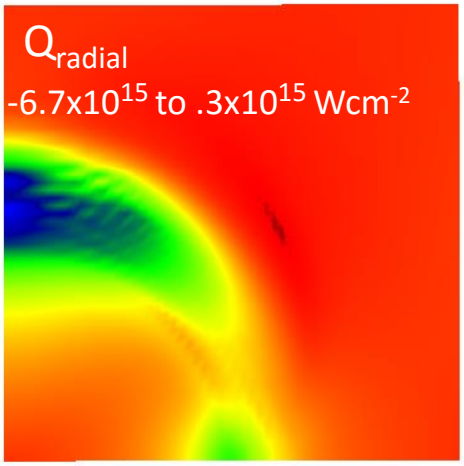

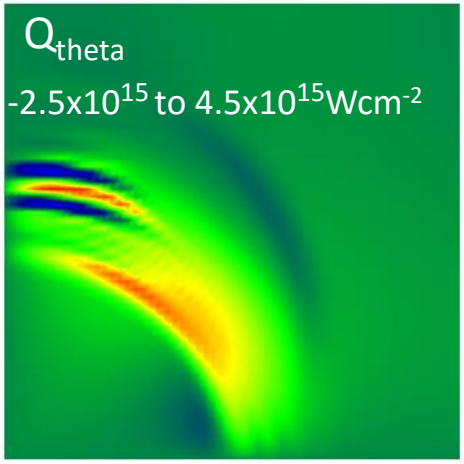

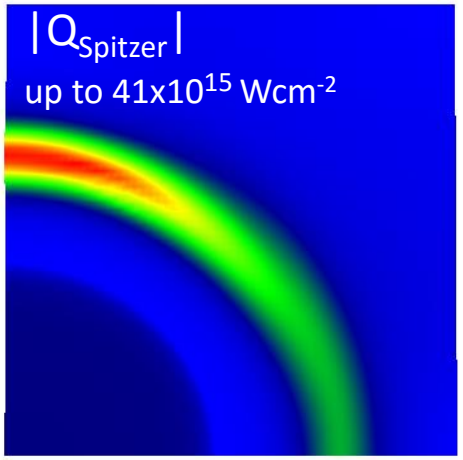

Possible collaborations

Reproducing astro-turbulence in lab

Opening up low density channels for fast ignition

Shock ignition: energy deposition and smoothing

Combined absorption/transport/instabilities in direct drive IFE

Improving VFP algorithms

Simple Vlasov code: 1D in space and velocity

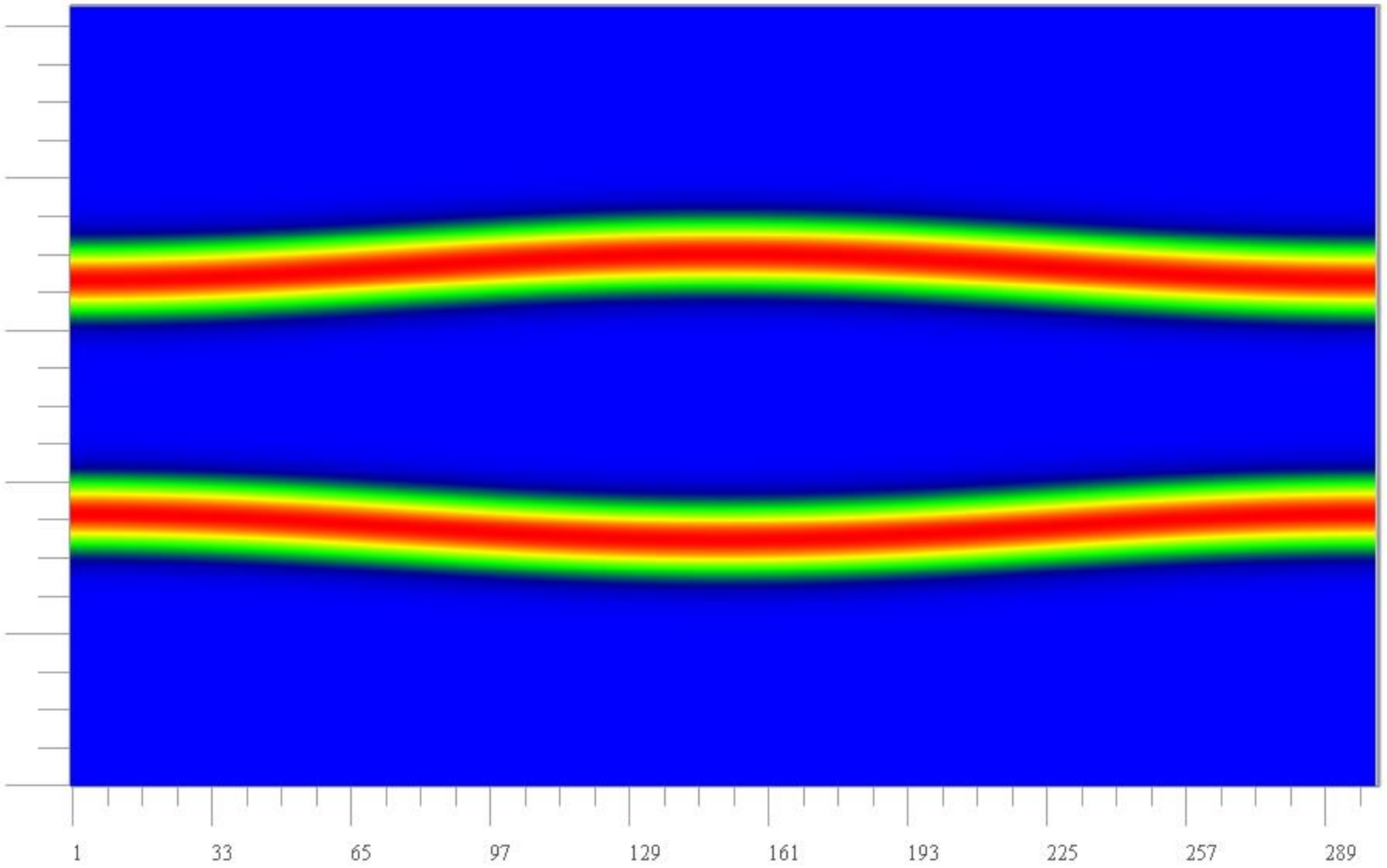
1
33
65
97
129
161
193
225
257
289
dim: 1

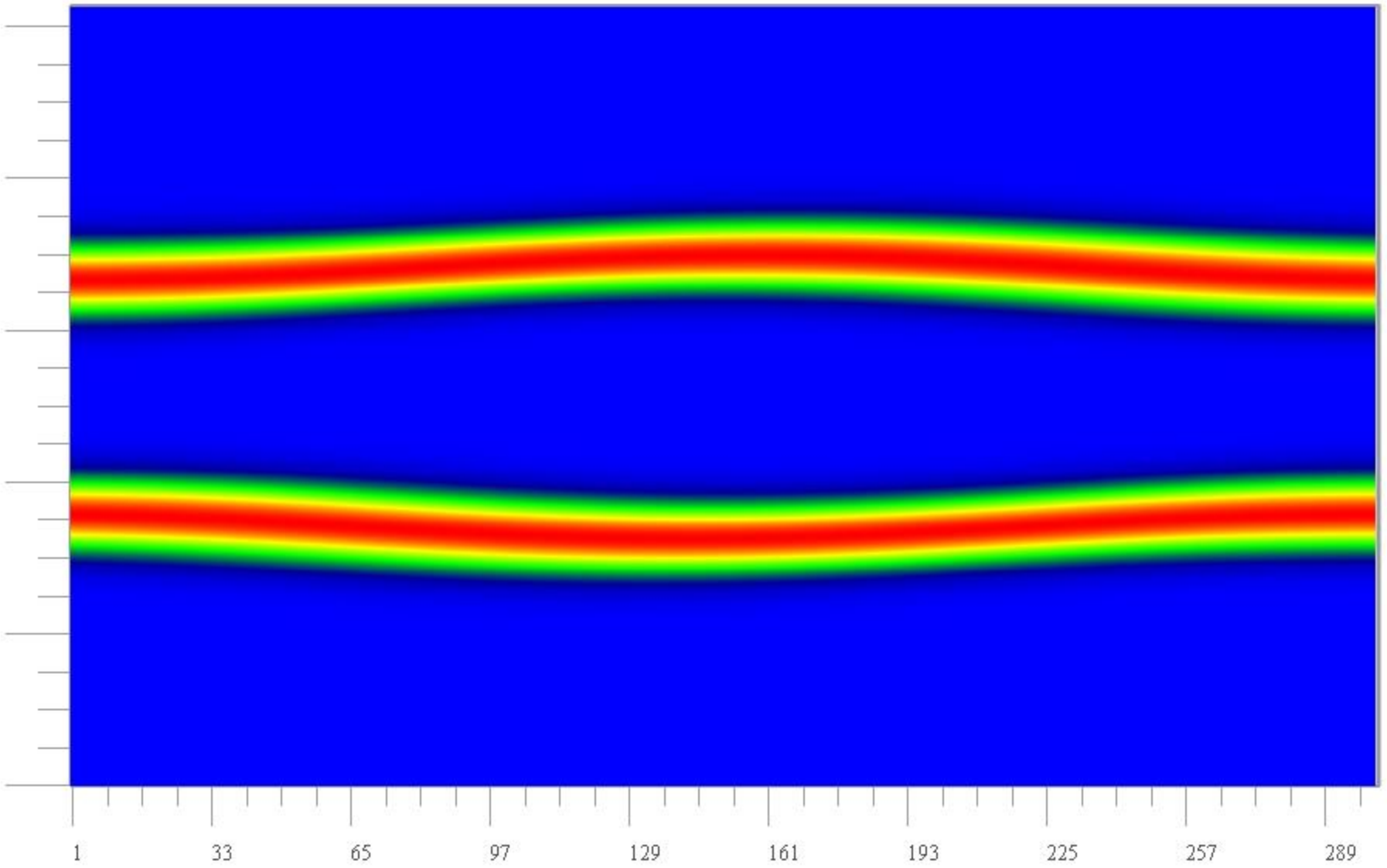
1
33
65
97
129
161
193
225
257
289
dim: 1

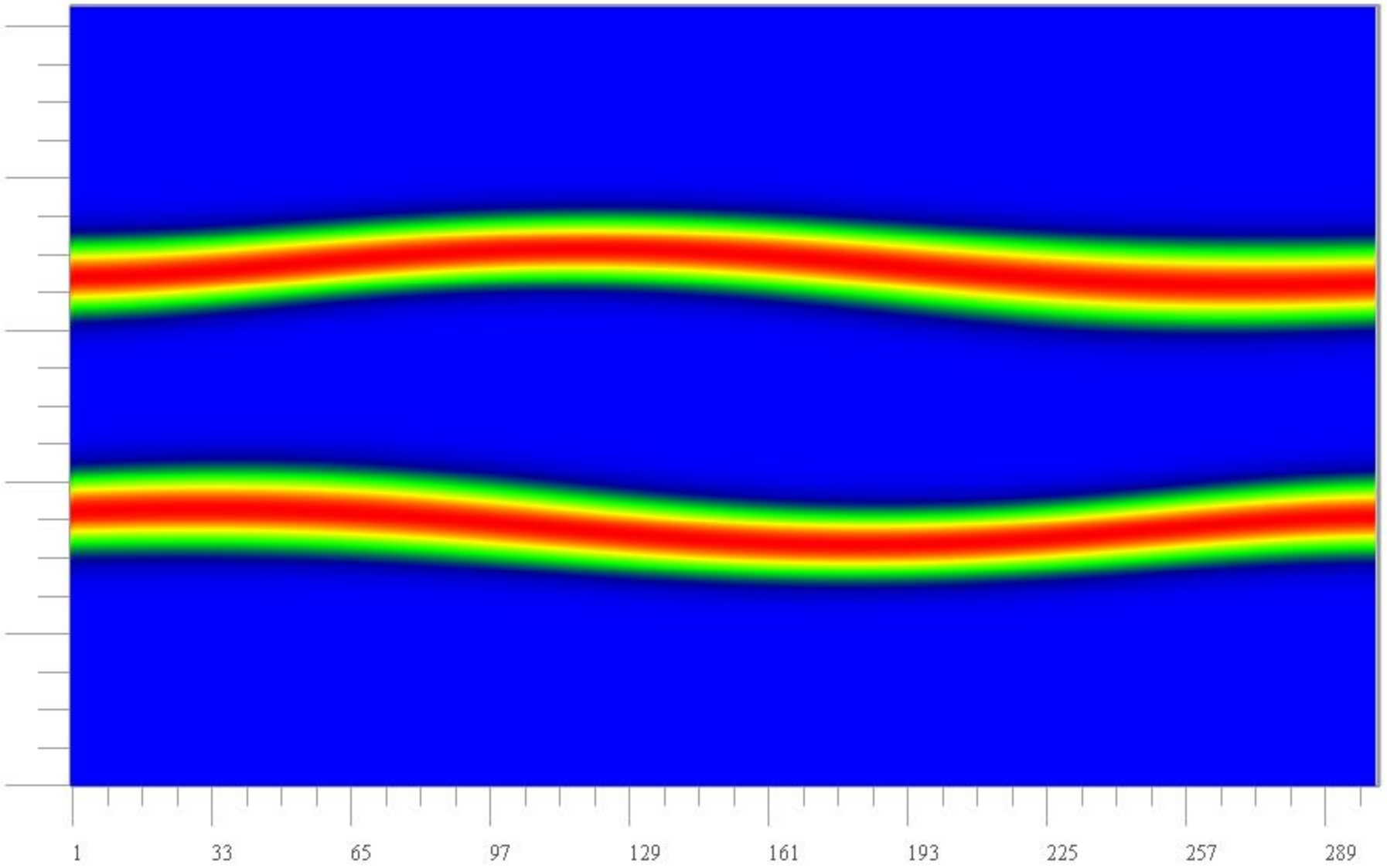
1
33
65
97
129
161
193
225
257
289
dim: 1

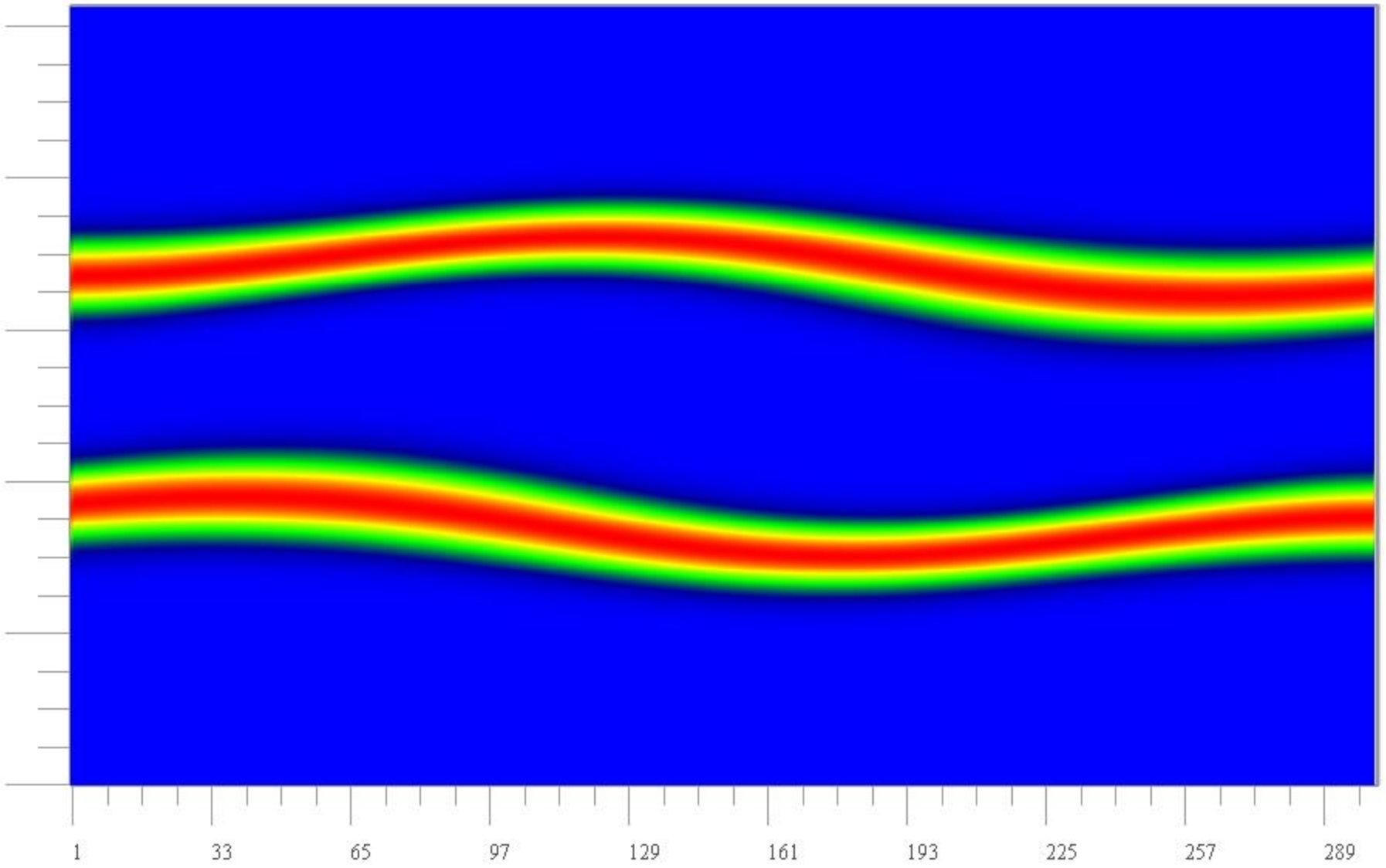
1
33
65
97
129
161
193
225
257
289
dim: 1

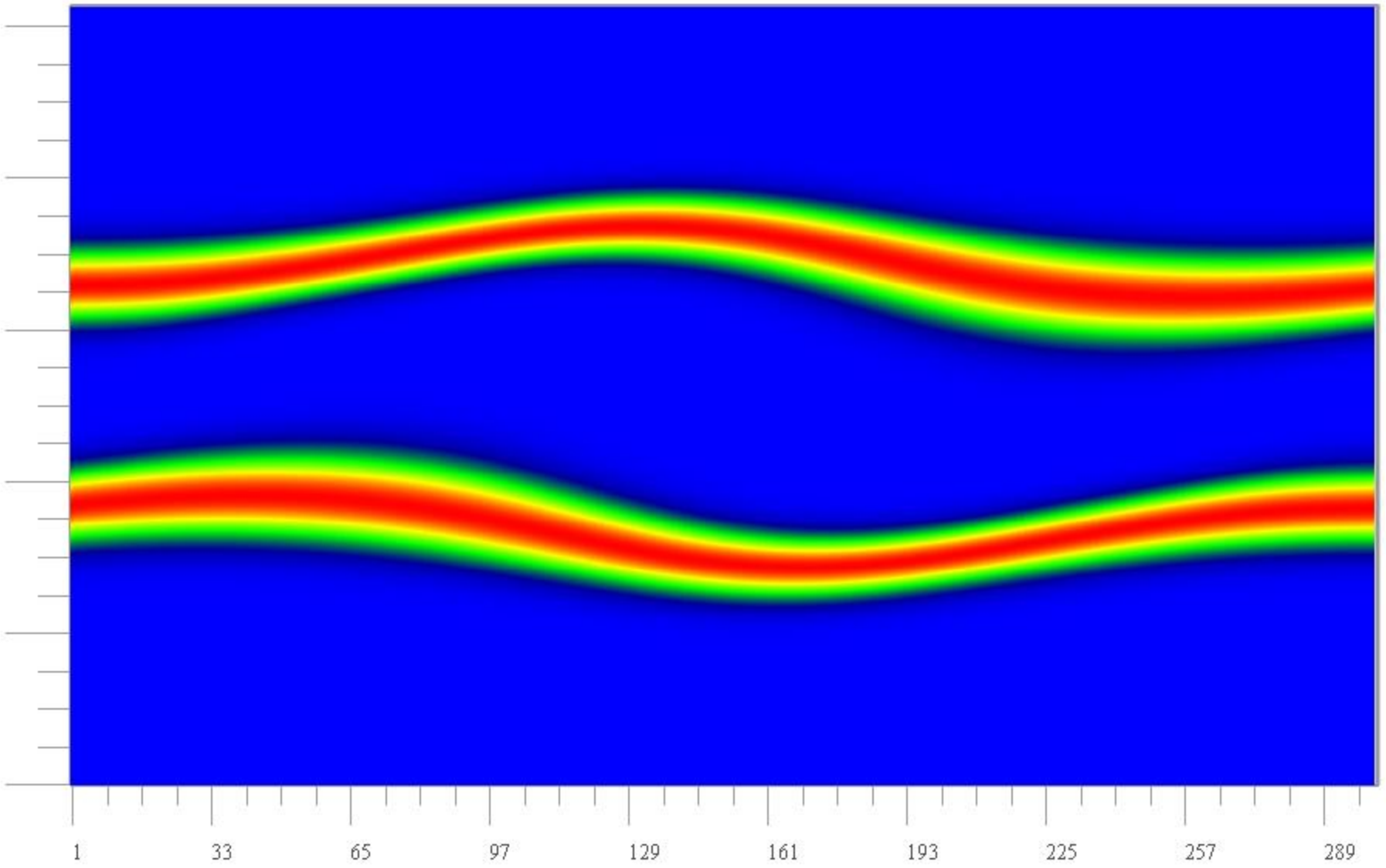
1
33
65
97
129
161
193
225
257
289
dim: 1

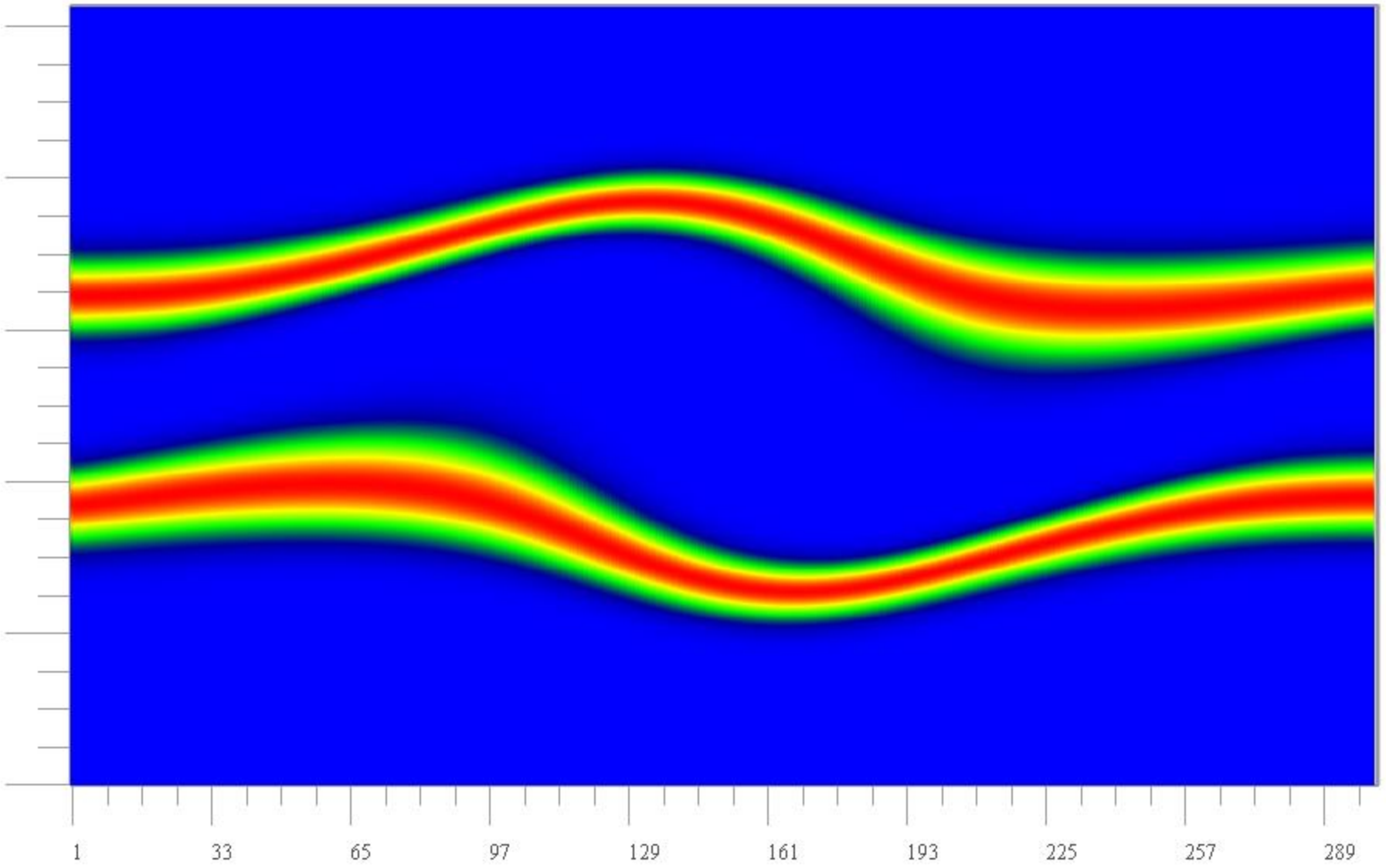
1
33
65
97
129
161
193
225
257
289
dim: 1

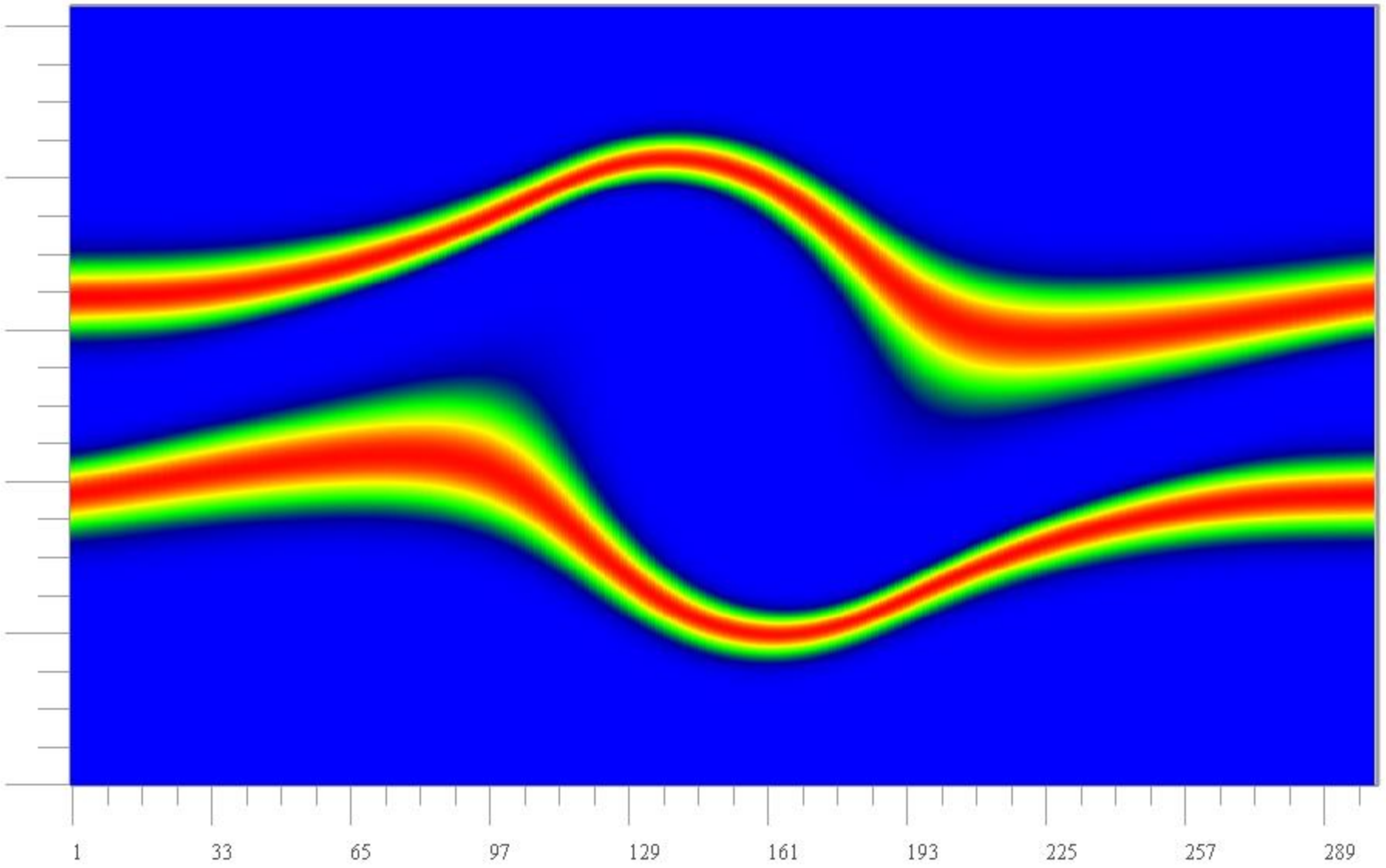
1
33
65
97
129
161
193
225
257
289
dim: 1

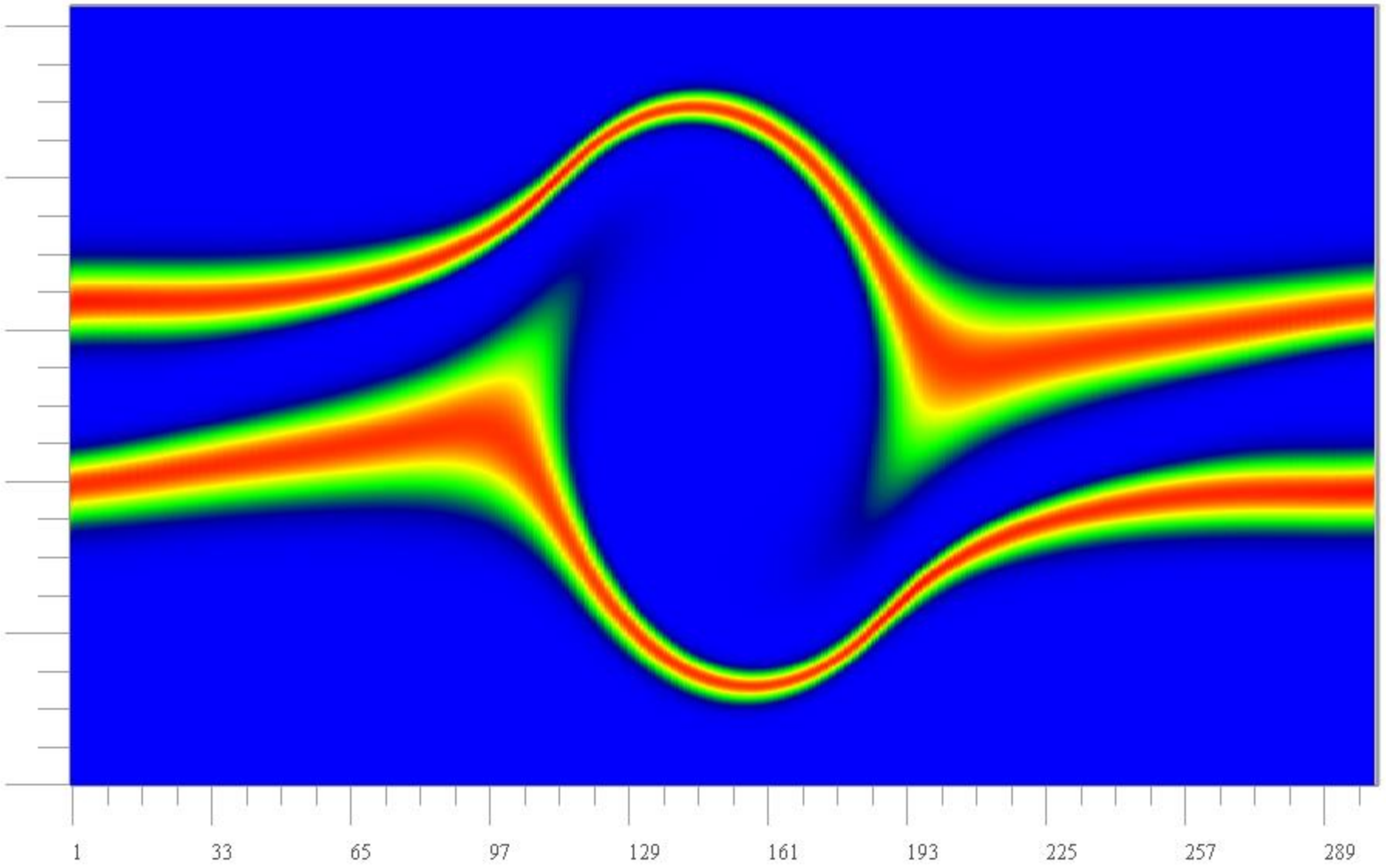
1
33
65
97
129
161
193
225
257
289
dim: 1

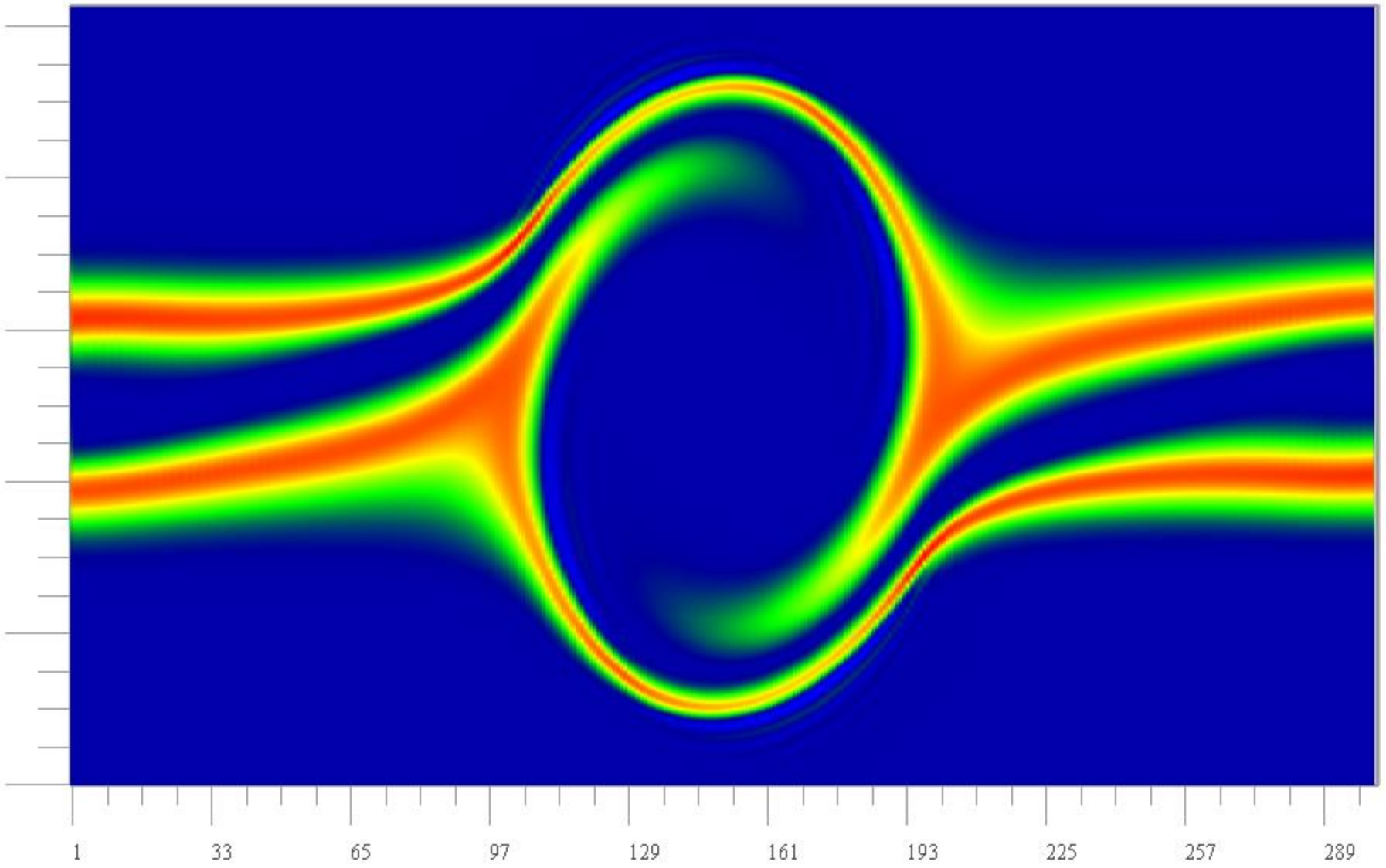
1
33
65
97
129
161
193
225
257
289
dim: 1

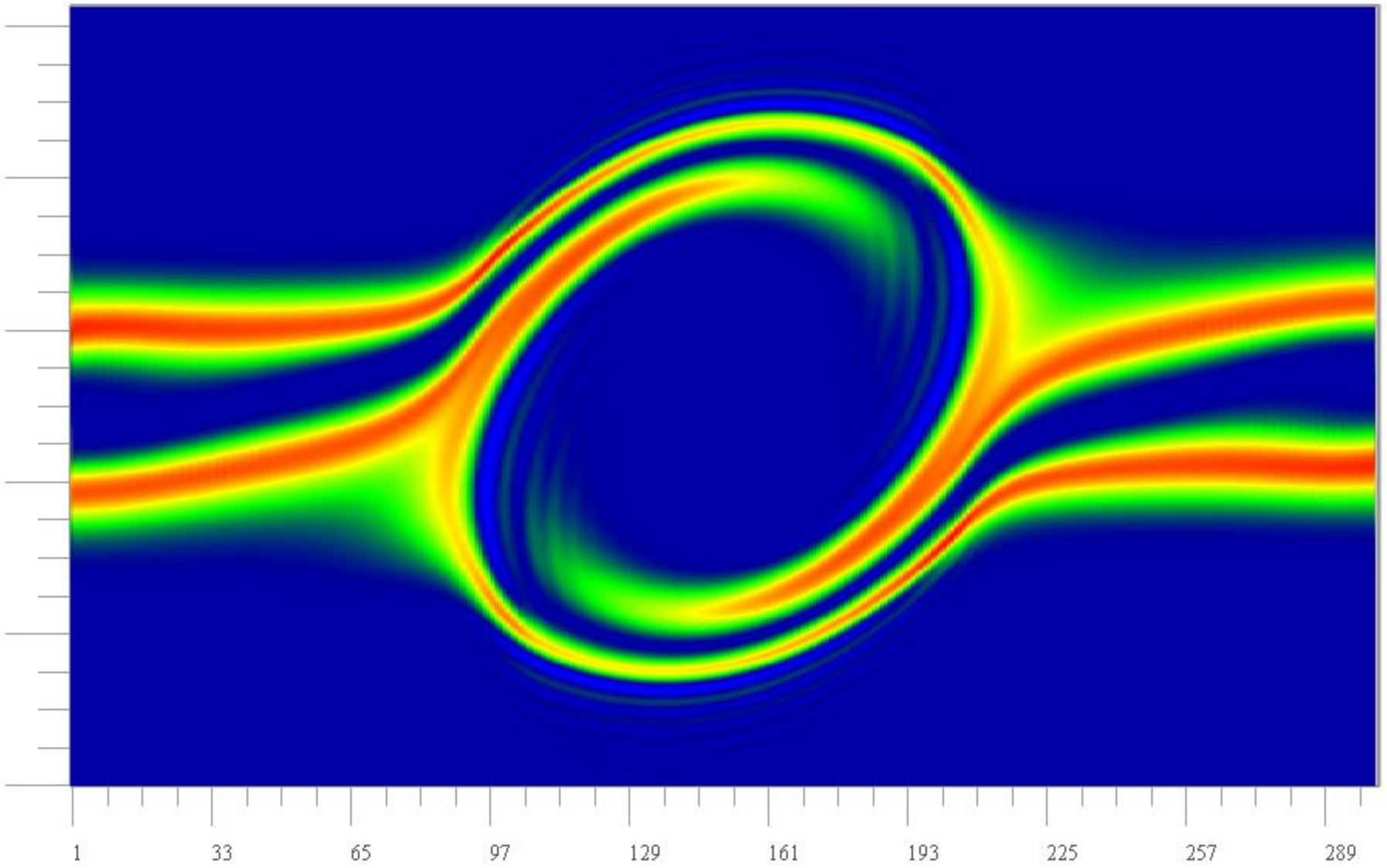
1
33
65
97
129
161
193
225
257
289
dim: 1

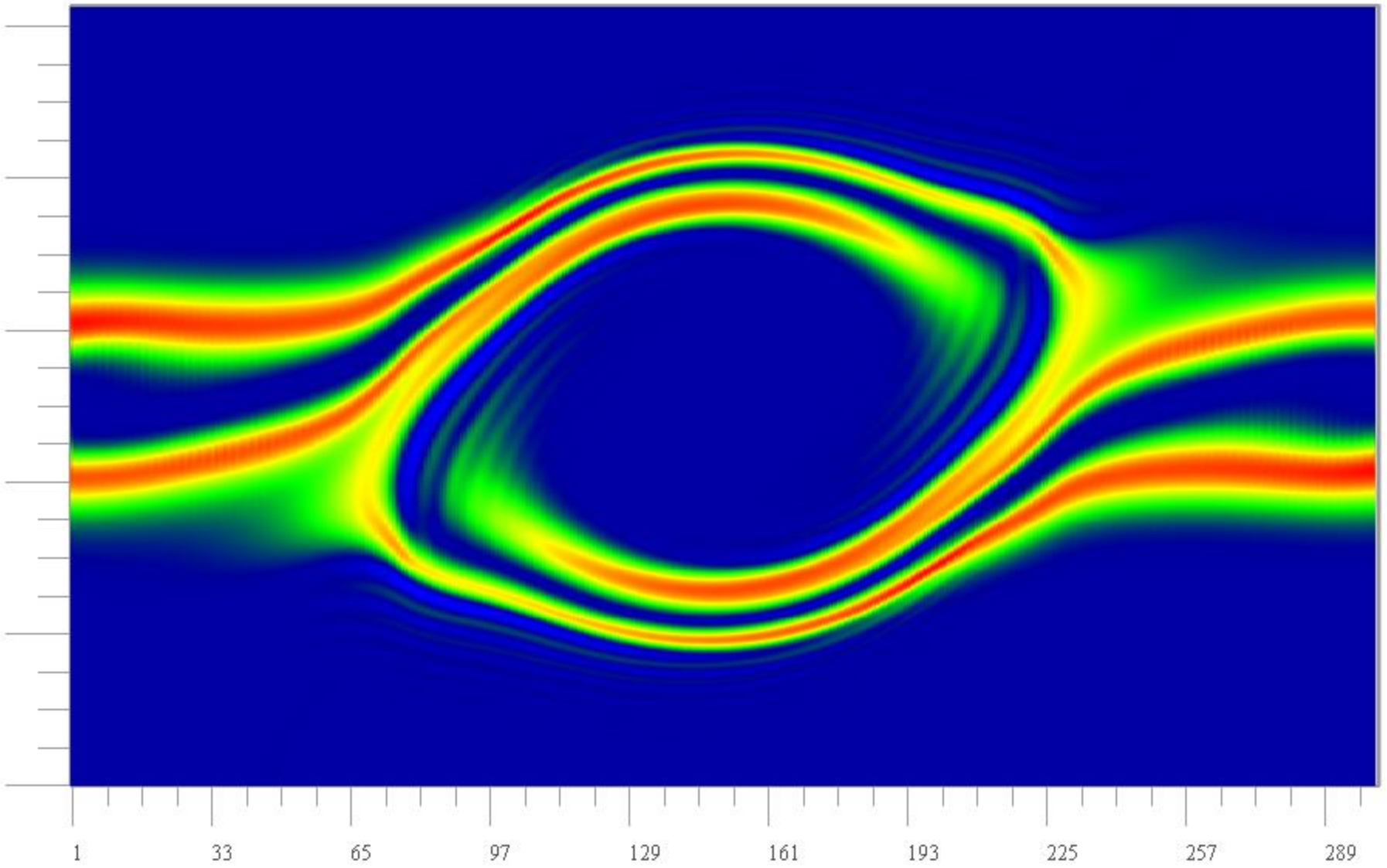
1
33
65
97
129
161
193
225
257
289
dim: 1

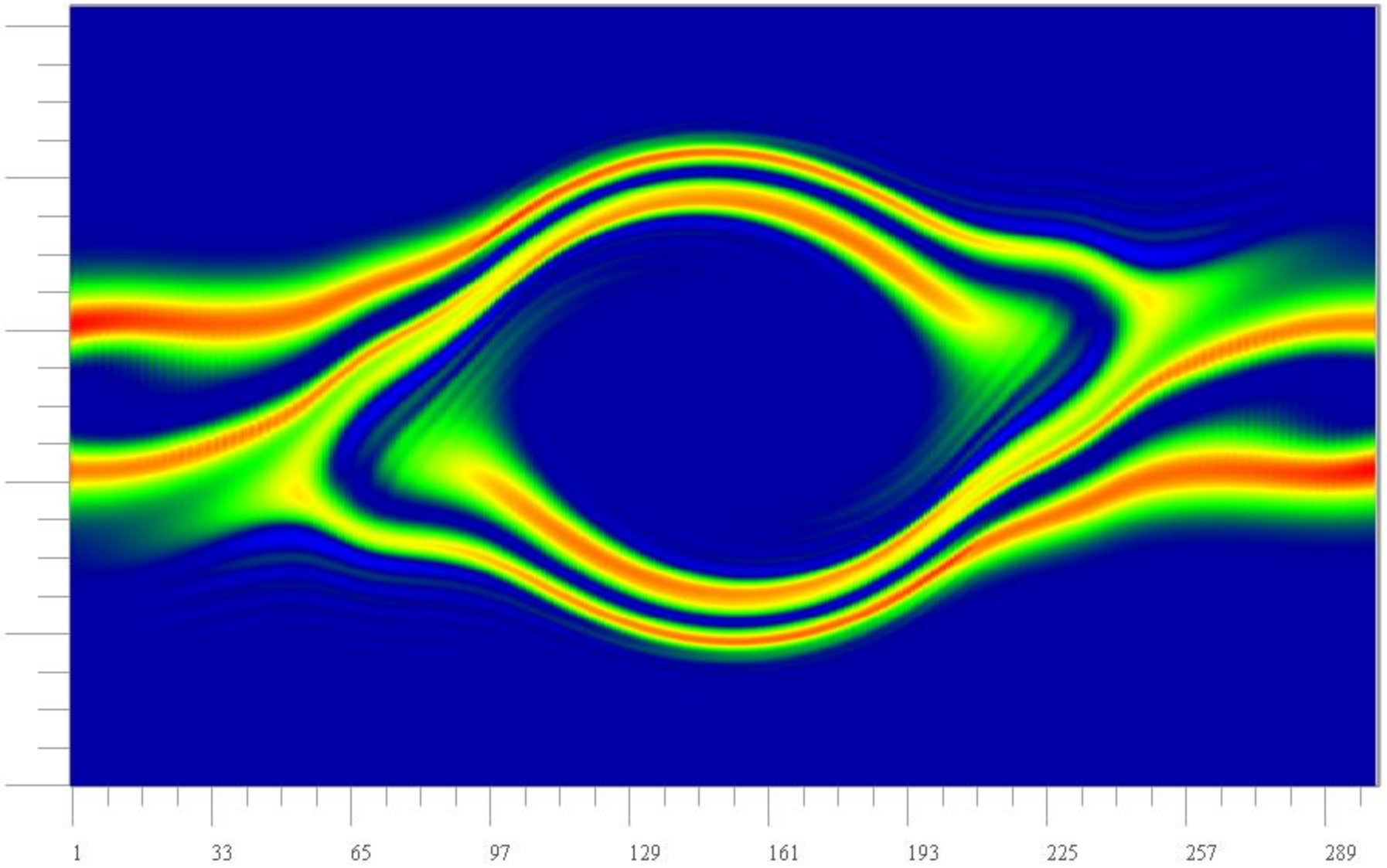
1
33
65
97
129
161
193
225
257
289
dim: 1

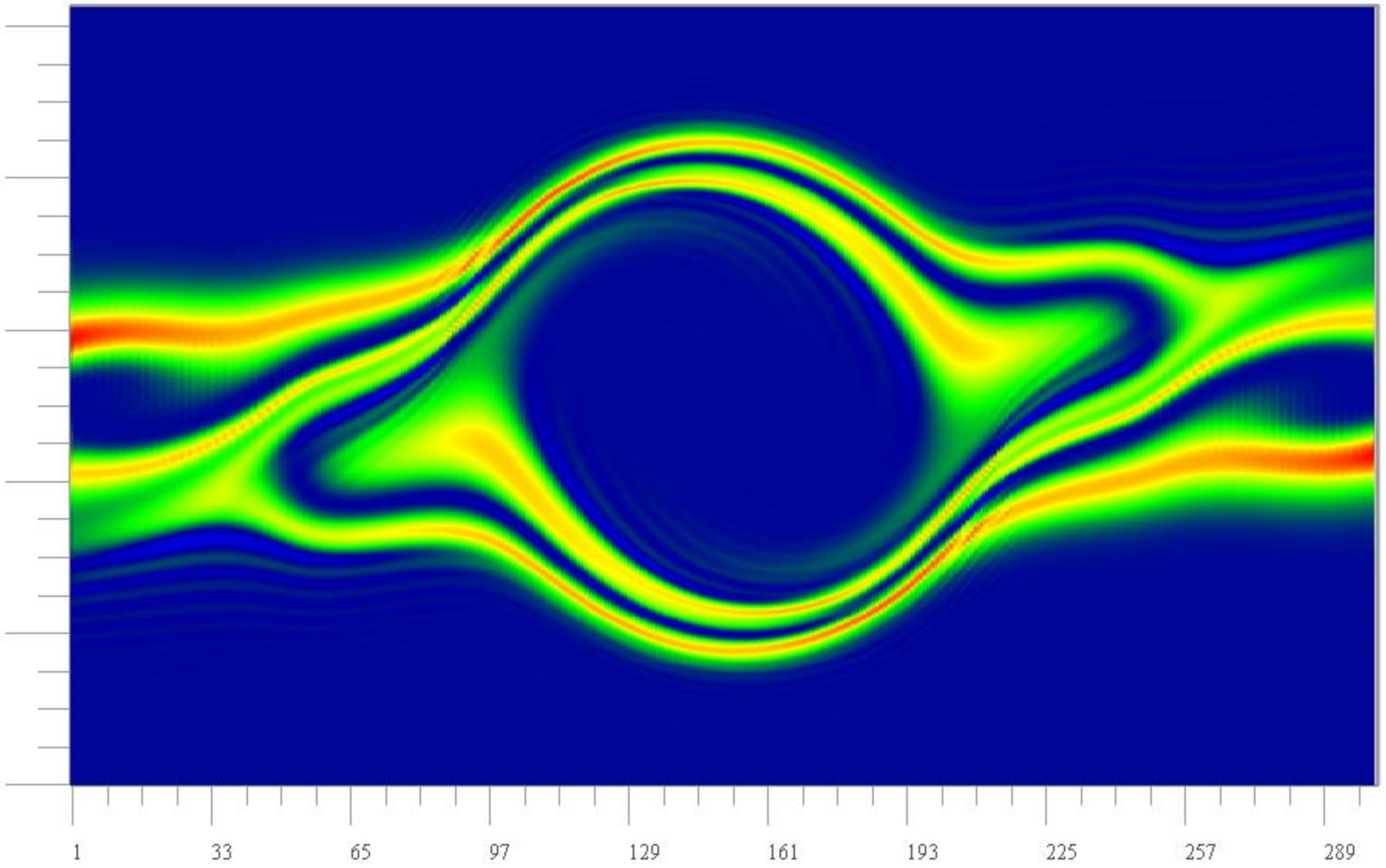
1
33
65
97
129
161
193
225
257
289
dim: 1

Possible collaborations

Reproducing astro-turbulence in lab

Opening up low density channels for fast ignition

Shock ignition: energy deposition and smoothing

Combined absorption/transport/instabilities in direct drive IFE

Improving VFP algorithms

VFP goes back a long way: ‘flux limitation’ (1981)
No combined model yet of (i) absorption (ii) transport (iii) instabilities

$$\frac{\partial f}{\partial t} + v_x \frac{\partial f}{\partial x} + E \frac{\partial f}{\partial v_x} = \left(\frac{\partial f}{\partial t}\right)_{\text{collision}},$$

$$\frac{\partial E}{\partial x} = r\left[\int f \, d^3v - 1\right].$$